JOURNAL OF PETROLOGY | VOLUME 44 | NUMBER 10 | PAGES 1833–1865 | 2003 | DOI: 10.1093/petrology/egg061

Cenozoic Volcanism in Tibet: Evidence for a Transition from Oceanic to Continental Subduction

LIN DING[1], PAUL KAPP[2]*, DALAI ZHONG[1] AND WANMING DENG[1]

[1]INSTITUTE OF GEOLOGY AND GEOPHYSICS, CHINESE ACADEMY OF SCIENCES, BEIJING 100029, PEOPLE'S REPUBLIC OF CHINA

[2]DEPARTMENT OF GEOSCIENCES, UNIVERSITY OF ARIZONA, TUCSON, AZ 85721-0077, USA

RECEIVED MARCH 15, 2002; ACCEPTED APRIL 14, 2003

Geochronological (K–Ar or $^{40}Ar/^{39}Ar$), major and trace element, Sr–Nd–Pb isotopic and mineral chemical data are presented for newly discovered Cenozoic volcanic rocks in the western Qiangtang and central Lhasa terranes of Tibet. Alkali basalts of 65–45 Ma occur in the western Qiangtang terrane and represent primitive mantle melts as indicated by high mg-numbers [$100 \times Mg/(Mg + Fe)$] (54–65), Cr (204–839 ppm) and Ni (94–218 ppm) contents, and relatively low ratios of $^{87}Sr/^{86}Sr$ (0·7046–0·7061), $^{206}Pb/^{204}Pb$ (18·21–18·89), $^{207}Pb/^{204}Pb$ (15·49–15·61) and $^{208}Pb/^{204}Pb$ (38·42–38·89), and high ratios of $^{143}Nd/^{144}Nd$ (0·5124–0·5127). In contrast, younger volcanic rocks in the western Qiangtang terrane (~30 Ma) and the central Lhasa terrane (~23, ~13 and ~8 Ma) are potassic to ultrapotassic and interpreted to have been derived from an enriched mantle source. They are characterized by very high contents of incompatible trace elements, negative Ta, Nb and Ti anomalies, and radiogenic Pb isotopic compositions ($^{206}Pb/^{204}Pb$ = 18·43–19·10; $^{207}Pb/^{204}Pb$ = 15·64–15·83; $^{208}Pb/^{204}Pb$ = 39·14–39·67). $^{87}Sr/^{86}Sr$ (0·7088–0·7092) and $^{143}Nd/^{144}Nd$ (~0·5122) ratios of the western Qiangtang terrane potassic lavas are similar to those of 45–29 Ma potassic volcanic rocks in the north–central Qiangtang terrane, whereas $^{87}Sr/^{86}Sr$ (0·7167–0·7243) and $^{143}Nd/^{144}Nd$ (~0·5119) ratios of central Lhasa terrane lavas are similar to those of 25–16 Ma ultrapotassic volcanic rocks in the western Lhasa terrane. The 65–45 Ma alkali basalts in the western Qiangtang terrane, along with widespread calc-alkaline volcanic rocks of this age in the Lhasa terrane, may be related to roll-back of a previously shallow north-dipping slab of Tethyan oceanic lithosphere beneath Tibet. Subduction as opposed to convective thinning of continental lithosphere is favored to explain potassic volcanism in Tibet because of its occurrence in distinct, east–west-trending belts (45–29 Ma in the Qiangtang terrane; 25–17 Ma in the northern Lhasa terrane; 16–8 Ma in the southern Lhasa terrane) and temporal and spatial relationships with major thrust systems.

KEY WORDS: *Tibet; geochemistry; Indo-Asian collision; sodic and potassic volcanism; continental subduction*

INTRODUCTION

The Tibetan plateau is commonly considered to be the archetypal collisional orogen; nevertheless, significant questions remain regarding its tectonic evolution. Perhaps the most fundamental is whether convergence between India and Asia was accommodated in the continental mantle lithosphere mainly by homogeneous thickening (e.g. Molnar *et al.*, 1993) or subduction (e.g. Tapponnier *et al.*, 2001). Geochemical, isotopic, and geochronological studies on Cenozoic volcanic rocks in Tibet, when integrated with constraints on the timing and distribution of crustal deformation, have the potential to address this question.

The oldest Cenozoic volcanic rocks that have been studied in detail in Tibet occur in the southern Lhasa terrane (Fig. 1). They are represented by the widespread and voluminous Linzizong Formation (Fig. 1), which ranges in age from 65 to 49 Ma near Lhasa (Maluski *et al.*, 1982; Xu *et al.*, 1985*a*; Coulon *et al.*,

*Corresponding author. Telephone: (520) 626-8763. E-mail: pkapp@geo.arizona.edu

Journal of Petrology 44(10) © Oxford University Press 2003; all rights reserved

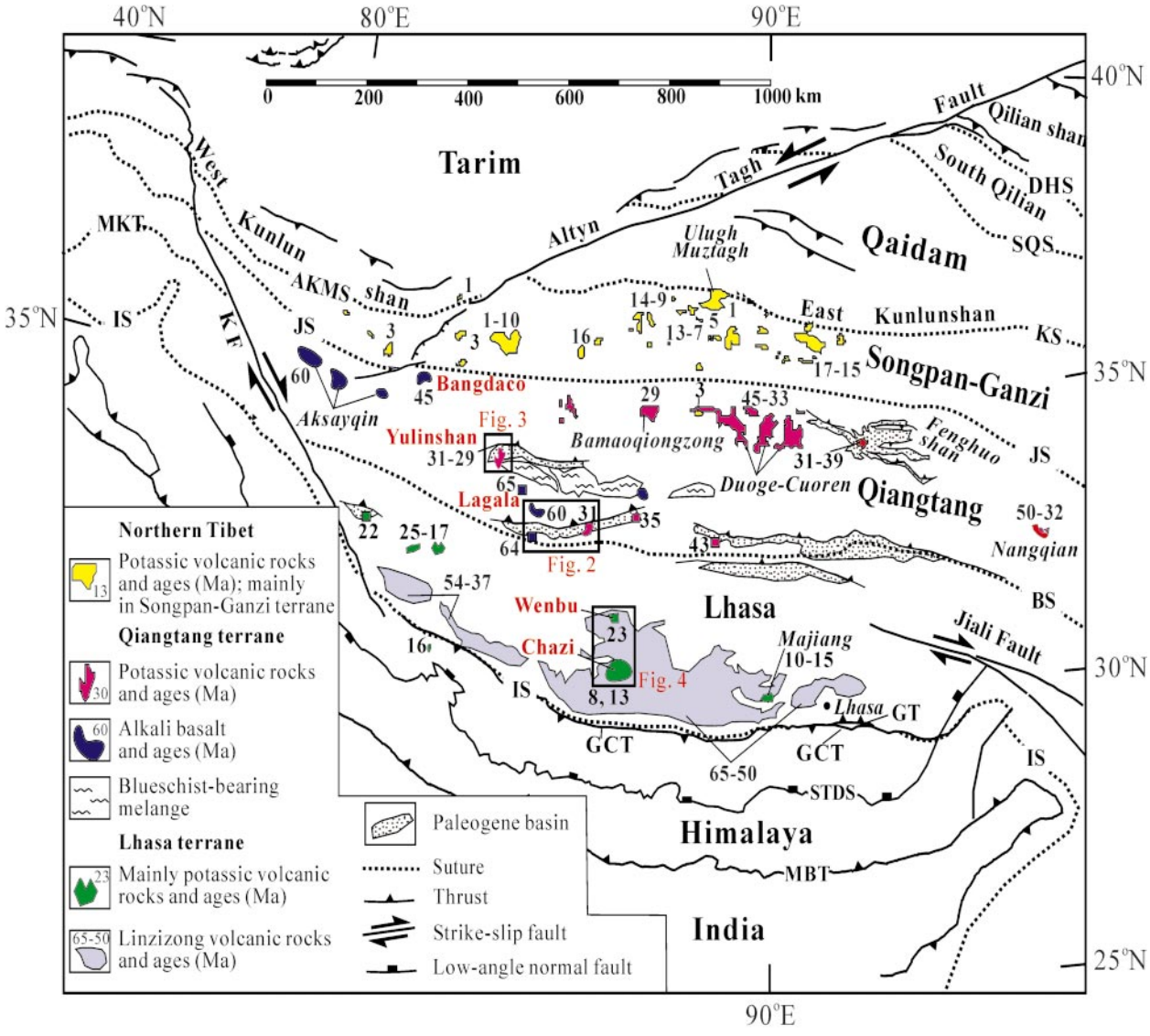

Fig. 1. Map of the Tibetan Plateau showing the major terranes and temporal–spatial distribution of Cenozoic volcanic rocks [modifed from Yin & Harrison (2000)]. Ages compiled from Coulon *et al.* (1986), Burchfiel *et al.* (1989), Deng (1989, 1998), Turner *et al.* (1996), Zheng *et al.* (1996), Chung *et al.* (1998), Miller *et al.* (1999, 2000), Deng *et al.* (2000), Hacker *et al.* (2000), Tan *et al.* (2000), Horton *et al.* (2002) and Kapp *et al.* (2002, 2003*a*). From north to south, the main suture zones between the terranes are: DHS, Danghe Nan Shan; SQS, Southern Qilian; KS, Kunlun; JS, Jinsha; BS, Bangong; IS, Indus. Major faults: GT, Gangdese thrust system; GCT, Great Counter thrust; STDS, Southern Tibet detachment system; MKT, Main Karakorum thrust; MBT, Main Boundary Thrust; KF, Karakoram fault.

1986; Zhou *et al.*, 2001) and from 54 to 37 Ma in southwestern Tibet (Miller *et al.*, 2000). Calc-alkaline granitoids of similar (Harrison *et al.*, 2000; Miller *et al.*, 2000), and even younger age (Miocene; D'Andrea *et al.*, 1999) have also been documented within the Gangdese (also referred to as Transhimalayan) batholith. Although significant uncertainty remains, it appears that the initiation age of Indo-Asian collision was between 70 and 50 Ma and diachronous along strike (younging from west to east) [see Yin & Harrison (2000) for discussion and references]. Igneous rocks older than the initiation age of Indo-Asian collision are attributed to north-dipping subduction of Tethyan oceanic lithosphere (e.g. Dewey & Bird, 1970; Coulon *et al.*, 1986; Debon *et al.*, 1986). The extent to which this oceanic subduction modified the structure of the Asian mantle lithosphere is poorly understood, in part because there are few constraints on how the dip-angle of the Tethyan slab changed with time. Also unclear is why calc-alkaline magmatism persisted in the southern

Lhasa terrane long after initiation of the Indo-Asian collision.

Potassic volcanic rocks are widely distributed across the Tibetan plateau and their ages span that of the Indo-Asian collision (50 Ma to Recent) (Fig. 1; see references in caption). Although substantial differences exist within and between localities, the lavas generally exhibit negative Nb, Ta and Ti anomalies, strong enrichment in incompatible elements, and relatively radiogenic Sr and Pb and unradiogenic Nd isotopic ratios. The latter characteristics are generally interpreted to indicate that parental magmas were derived from an enriched continental mantle source that was isolated from convecting asthenosphere since at least Proterozoic time (e.g. Turner *et al.*, 1996), although the possibility of a contribution from a mafic granulitic or eclogitic lower-crustal source has been raised (Hacker *et al.*, 2000; Cooper *et al.*, 2002).

The two most widely proposed mechanisms to explain the genesis of Tibetan potassic volcanism are: (1) mantle melting following rapid removal of large portions of previously thickened and therefore gravitationally unstable mantle lithosphere (Molnar *et al.*, 1993; Turner *et al.*, 1993, 1996; Chung *et al.*, 1998; Miller *et al.*, 1999; Williams *et al.*, 2001); (2) melting related to intracontinental subduction (Deng, 1991; Arnaud *et al.*, 1992; Meyer *et al.*, 1998; Tapponnier *et al.*, 2001; Wang *et al.*, 2001). The first mechanism predicts that potassic magmatism should be regionally widespread and postdate major crustal shortening (e.g. Houseman *et al.*, 1981), whereas the second mechanism predicts that there should be distinct belts of magmatism in the hinterlands of major thrust systems, with magmatism being coeval with thrusting. More recently, models involving slab break-off (DeCelles *et al.*, 2002; Kohn & Parkinson, 2002; Maheo *et al.*, 2002) and decompression melting during extension/transtension and concomitant mantle attenuation (Wang *et al.*, 2001; Cooper *et al.*, 2002) have been put forward. They can be placed into the end-member subduction vs distributed deformation models for the continental mantle lithosphere, and also make distinct predictions regarding the temporal and spatial relationships between volcanism and deformation.

Additional constraints on the age, distribution and petrology of Cenozoic volcanic rocks in Tibet, especially those within the poorly studied plateau interior, are necessary to distinguish between the different tectonic models for their petrogenesis. Detailed studies on earliest Tertiary volcanic rocks are restricted to the southern Lhasa terrane. It is unclear whether a recently defined belt of Eocene–Oligocene potassic volcanic rocks and high-K calc-alkaline granitoids in the eastern Qiangtang terrane (Chung *et al.*, 1998; Roger *et al.*, 2000) extends westward across the Tibetan plateau; only two localities of Eocene–Oligocene volcanic rocks have been studied in detail in the Qiangtang terrane of central Tibet (Duoge-Cuoren and Bamaoqiongzong; Fig. 1; Deng, 1993, 1998; Hacker *et al.*, 2000; Tan *et al.*, 2000). Likewise, it is uncertain whether 25–16 Ma volcanic rocks in westernmost Tibet (Turner *et al.*, 1996; Miller *et al.*, 1999) and 15–10 Ma volcanic rocks near Lhasa (Majiang; Fig. 1; Coulon *et al.*, 1986) are spatially restricted or part of much more extensive east–west-trending belts.

This paper presents results of field, geochronological, geochemical and isotopic studies of Cenozoic volcanic rocks in the western Qiangtang and central Lhasa terranes. They provide the first documentation of ~60 Ma alkali basalts and ~30 Ma potassic volcanic rocks in the western Qiangtang terrane and ~23, ~13 and ~8 Ma potassic to ultrapotassic volcanic rocks in the central Lhasa terrane. The geochemical and isotopic characteristics of these volcanic rocks are compared with those of previously studied volcanic rocks in Tibet. A tectonic model is presented for the petrogenesis of Cenozoic magmatism, which integrates recent constraints on the crustal deformation history and present-day mantle structure of Tibet.

GEOLOGICAL BACKGROUND

From north to south, the interior of the Tibetan plateau comprises the roughly east–west-trending Songpan–Ganzi, Qiangtang and Lhasa terranes (Fig. 1; e.g. Chang & Zheng, 1973; Dewey *et al.*, 1988; Yin & Harrison, 2000). The Songpan–Ganzi terrane comprises the largest volume of Triassic strata on Earth ($2{\cdot}2 \times 10^6$ km^3; Nie *et al.*, 1994). These strata include multi-kilometer-thick sequences of Late Triassic flysch (Rao *et al.*, 1987; Liu, 1988; Hou *et al.*, 1991) that were deposited variably on continental (Burchfiel *et al.*, 1995; Zhou & Graham, 1996) and oceanic crust (Sengör, 1987), and were derived mostly from the Triassic Qinling–Dabie orogen to the NE (Nie *et al.*, 1994; Yin & Nie, 1996; Zhou & Graham, 1996; Bruguier *et al.*, 1997). The change from marine to nonmarine sedimentation within the Songpan–Ganzi terrane during the earliest Jurassic is taken to record final accretion of the Qiangtang terrane to the Eurasian margin following ocean closure along the Late Triassic–Early Jurassic Jinsha suture by south-dipping subduction (Pearce & Mei, 1988; Yin & Harrison, 2000), north-dipping subduction (Coward *et al.*, 1988; Li *et al.*, 1995), or both (Leeder *et al.*, 1988). The Songpan–Ganzi terrane and Jinsha suture have been modified significantly by major Tertiary thrust systems and associated non-marine basins of primarily Eocene–Oligocene age (e.g. Coward *et al.*, 1988; Wang *et al.*, 2002). Cenozoic volcanic rocks in

the Songpan–Ganzi terrane are volumetrically minor but widely distributed (Fig. 1), mainly mafic–potassic to ultrapotassic in composition, and range in age from 17 Ma to Recent (Deng, 1989; Turner *et al.*, 1993, 1996; Zheng *et al.*, 1996; Cooper *et al.*, 2002). An exception is in the Ulugh Muztagh area (Fig. 1), where ~4 Ma rhyolites have been documented (Burchfiel *et al.*, 1989; McKenna & Walker, 1990).

In the central Qiangtang terrane, a >500 km long east–west belt of blueschist-bearing mélange (Fig. 1) lies structurally beneath Paleozoic to Mesozoic, mainly shallow marine, strata in the footwall of major Late Triassic–Early Jurassic domal low-angle normal faults (Kapp *et al.*, 2000). The mélange is interpreted to represent either a distinct suture zone separating a northern Qiangtang terrane of Cathaysian affinity from a southern Qiangtang terrane of Gondwanan affinity (Li *et al.*, 1995) or materials that were thrust beneath the Qiangtang terrane during early Mesozoic south-dipping oceanic subduction along the Jinsha suture and then exhumed in an intracontinental setting by Late Triassic–Early Jurassic normal faulting (Kapp *et al.*, 2000, 2003*b*). Early Tertiary (60–45 Ma) alkali basalts occur in the Aksayqin area of the northwestern-most Qiangtang terrane and overlie Cretaceous marine limestone (Deng, 1998). East–west-trending Paleogene non-marine basins are widely distributed across the Qiangtang terrane. They contain a fill of fluvial sandstone and conglomerate, and lacustrine limestone and mudstone, that ranges from Paleocene to Oligocene in age based on biostratigraphic studies and K–Ar (Wang *et al.*, 1983; Xu *et al.*, 1985*b*; Cheng & Xu, 1986) and $^{40}Ar/^{39}Ar$ (Kapp *et al.*, 2002) dating of interbedded volcanic rocks. The Paleogene basins are in most places bounded on their northern margins by north-dipping thrust faults (Lei *et al.*, 1996; Luo *et al.*, 1996; Kapp *et al.*, 2000, 2002, 2003*b*). Eocene–Early Oligocene (50–29 Ma) potassic to ultrapotassic volcanic and subordinate intrusive rocks are widely distributed throughout the Qiangtang terrane (Fig. 1 and references in caption).

The Lhasa terrane and at least the southern portion of the Qiangtang terrane were contiguous along the margin of Gondwana during late Paleozoic time (Yin *et al.*, 1988; Li & Zheng, 1993). Rifting of the Qiangtang terrane from the Lhasa terrane, and opening of the intervening Bangong ocean, occurred during Permo-Triassic (Sengör, 1984) or Early Jurassic (Yin *et al.*, 1988) time. Subsequent closure of the ocean along the Bangong suture occurred by northward subduction beneath the Qiangtang terrane and perhaps one or more oceanic island arc terranes during Middle Jurassic to Early Cretaceous time (Girardeau *et al.*, 1984; Tang & Wang, 1984; Pearce & Deng, 1988). Ocean closure was followed by major Early Cretaceous continental collision between the Lhasa and Qiangtang terranes (Murphy *et al.*, 1997). Localized Tertiary thrusts and associated Paleocene to Oligocene non-marine basin fill along the Bangong suture (Coward *et al.*, 1988; Leeder *et al.*, 1988; Yin & Harrison, 2000; Kapp *et al.*, 2002, 2003*a*) suggest that this collision may have continued during Paleogene time.

Granitoids in the Lhasa terrane have been divided into two belts: the mainly dioritic Cretaceous–Tertiary Gangdese (Transhimalaya) plutonic belt in the southern Lhasa terrane, and a belt in the northern Lhasa terrane that includes Early Cretaceous peraluminous granites (Xu *et al.*, 1985*a*; Harris *et al.*, 1990). Emplacement of the Gangdese batholith is attributed to northward subduction of Tethyan oceanic lithosphere beneath the southern Lhasa terrane, along the Indus suture, before collision with India at ~50 Ma (e.g. Dewey & Bird, 1970; Tapponnier *et al.*, 1981; Allègre *et al.*, 1984; Debon *et al.*, 1986). Magmatism of similar geochemistry to pre-50 Ma batholith rocks (high-K calc-alkaline) continued in the Gangdese belt until Late Miocene time, suggesting that fluid and thermal conditions typical of arc-type settings persisted in the southern Lhasa terrane >40 Myr after initiation of Indo-Asian collision (D'Andrea *et al.*, 1999; Miller *et al.*, 1999; Harrison *et al.*, 2000). The petrogenesis of the northern Lhasa terrane belt has been attributed to: (1) crustal anatexis during Lhasa–Qiangtang continental collision (Xu *et al.*, 1985*a*; Pearce & Mei, 1988); (2) high-temperature crustal anatexis related to asthenospheric upwelling and mantle attenuation (Harris *et al.*, 1990); (3) low-angle, northward-dipping subduction of the Tethyan oceanic lithosphere (Coulon *et al.*, 1986).

The Linzizong Formation is widely distributed in the southern half of the Lhasa terrane and consists of up to 2500 m of calc-alkaline andesitic flows, tuffs and breccias, and dacitic to rhyolitic ignimbrites (Wang, 1980; Coulon *et al.*, 1986; Pearce & Mei, 1988; Miller *et al.*, 2000; Zhou *et al.*, 2001; Dong, 2002). Near Lhasa, the volcanic rocks are between 60 and 49 Ma and are locally intruded by the ~53 Ma Lhasa granite (Maluski *et al.*, 1982; Xu *et al.*, 1985*a*; Coulon *et al.*, 1986). In SW Tibet, the volcanic rocks tend to be younger (54–37 Ma; Miller *et al.*, 2000). Additional, poorly studied volcanic sequences of latest Cretaceous–earliest Tertiary age extend into the northern Lhasa terrane (Liu, 1988; Murphy *et al.*, 1997) and across the Bangong suture zone (Kapp *et al.*, 2002). Throughout much of the southern Lhasa terrane, the gently folded Linzizong Formation rests unconformably on strongly deformed Cretaceous and older rocks (e.g. Tapponnier *et al.*, 1981; Burg *et al.*, 1983; Allègre *et al.*, 1984; Burg & Chen, 1984; Pan, 1993; Murphy *et al.*, 1997). This relationship demonstrates that upper-crustal

shortening in the Lhasa terrane largely pre-dates the Indo-Asian collision, at least where Linzizong volcanic rocks are preserved (Fig. 1). However, to the south, the Indus suture zone was strongly modified by the Late Oligocene (30–23 Ma) north-dipping Gangdese thrust system and the Miocene (19–10 Ma) south-dipping Great Counter thrust system (Yin *et al.*, 1994; Quidelleur *et al.*, 1997; Yin *et al.*, 1999*a*; Harrison *et al.*, 2000). Cenozoic potassic to ultrapotassic volcanic rocks have been documented previously only in the western Lhasa terrane (25–16 Ma; Turner *et al.*, 1996; Miller *et al.*, 1999) and in the Majiang area near Lhasa (15–10 Ma; Coulon *et al.*, 1986).

Despite continuing convergence between India and Asia, active deformation of the Tibetan plateau interior is characterized by roughly north-striking normal fault systems and kinematically linked strike-slip faults (Tapponnier & Molnar, 1977; Armijo *et al.*, 1986, 1989; Yin *et al.*, 1999*b*; Taylor *et al.*, 2003). There appears to be a gradual change from normal-fault-dominated to strike-slip-dominated deformation from south to north across the plateau. Rift systems in the Lhasa and Qiangtang terranes are suggested to have initiated between 14 and 4 Ma (Coleman & Hodges, 1995; Harrison *et al.*, 1995; Yin *et al.*, 1999*b*; Blisniuk *et al.*, 2001).

The Tibetan lithosphere exhibits major north–south variations in structure and geophysical properties (Zhao *et al.*, 1993; Hirn *et al.*, 1995; Nelson *et al.*, 1996; Owens & Zandt, 1997; Kosarev *et al.*, 1999; Kind *et al.*, 2002).The crustal thickness decreases south to north, from 80–70 km in the Lhasa terrane to ~65 km in the Qiangtang terrane, and to 65–55 km in the Songpan–Ganzi terrane (Nelson *et al.*, 1996; Owens & Zandt, 1997; Zhao *et al.*, 2001; Kind *et al.*, 2002). Analysis of teleseismic P waves suggests that Indian mantle lithosphere may have underthrust beneath southern Tibet to as far north as the Bangong suture (Fig. 1), where it appears to be subducting steeply (Owens & Zandt, 1997; Kosarev *et al.*, 1999). In contrast to southern Tibet, the northern Qiangtang and Songpan–Ganzi terranes are characterized by an upper mantle with inefficient S-wave propagation and low P-wave velocities (e.g. Bird & Toksoz, 1977; Chen & Molnar, 1981; Brandon & Romanowicz, 1986). In addition, the north–central Tibetan crust exhibits anomalously high Poisson's ratios and zones of low seismic velocities (Owens & Zandt, 1997). The geophysical properties of north–central Tibet have been interpreted to reflect the presence of partial melts within both the crust and mantle (Owens & Zandt, 1997; Wei *et al.*, 2001). Both Deng (1998) and Hacker *et al.* (2000) suggested that the lower crust (50–30 km depth) of the Qiangtang terrane is composed of anhydrous metasedimentary and mafic granulites based on studies of xenoliths in Cenozoic volcanic rocks. Supracrustal lithologies could have been emplaced into the lower crust of the northern Qiangtang terrane by southward flat-slab oceanic subduction along the Jinsha suture during early Mesozoic time (Kapp *et al.*, 2000) and major Tertiary underthrusting along reactivated Mesozoic suture zones (Hacker *et al.*, 2000; Yin & Harrison, 2000; Tapponnier *et al.*, 2001).

CENOZOIC VOLCANIC ROCKS IN WESTERN QIANGTANG AND CENTRAL LHASA TERRANES

Paleocene to Middle Eocene volcanic rocks were studied at two localities within the western Qiangtang terrane. Lagala basaltic lavas are located ~40 km north of the Bangong suture and extend over 50 km^2 (Figs 1 and 2). They crop out as low-relief hills and were emplaced onto Jurassic flysch and limestone. Grey–white sandstones have been baked to a brick-red colour where they are in contact with the lava flows. In the Bangdaco area, ~200 km north of the Bangong suture (Fig. 1), is a small flat-lying basaltic lava sheet that lies unconformably on Cretaceous marine limestone. The Cretaceous limestone is strongly folded and occurs to the north along the Jinsha suture zone in the footwall of a north-dipping thrust, with upper Paleozoic sandstone and limestone in the hanging wall. Similar basaltic flows, ~150 km along strike to the west in the Aksayqin area (Fig. 1), have been dated at 60–45 Ma by K–Ar and $^{40}Ar/^{39}Ar$ methods (Deng, 1998).

Flows of ultrapotassic basaltic trachyandesite, trachyandesite and trachyte have previously been reported to be interbedded with nonmarine sandstone and conglomerate within the Paleogene Kangtuo basin of the southwestern Qiangtang terrane (Fig. 2). The volcanic rocks have been dated at ~31 Ma by the K–Ar method (no uncertainty provided; Cheng & Xu, 1986). This paper reports results from a newly discovered locality of Early Oligocene potassic volcanic rocks within the Yulinshan area of the west–central Qiangtang terrane (Figs 1 and 3). The volcanic rocks consist of sheeted lavas that erupted over an area of ~200 km^2 and conformably overlie red non-marine conglomerate and sandstone. Three distinct lava sheets, separated by two weathered horizons, have been recognized (Fig. 3): the oldest is a sequence of basaltic trachyandesite and trachyandesite; the second consists of leucite tephriphonolite, trachyandesite and trachyte; the youngest consists of trachyte. The sedimentary basin fill and volcanic rocks are broadly folded, and ~10 km north of the Yulinshan area,

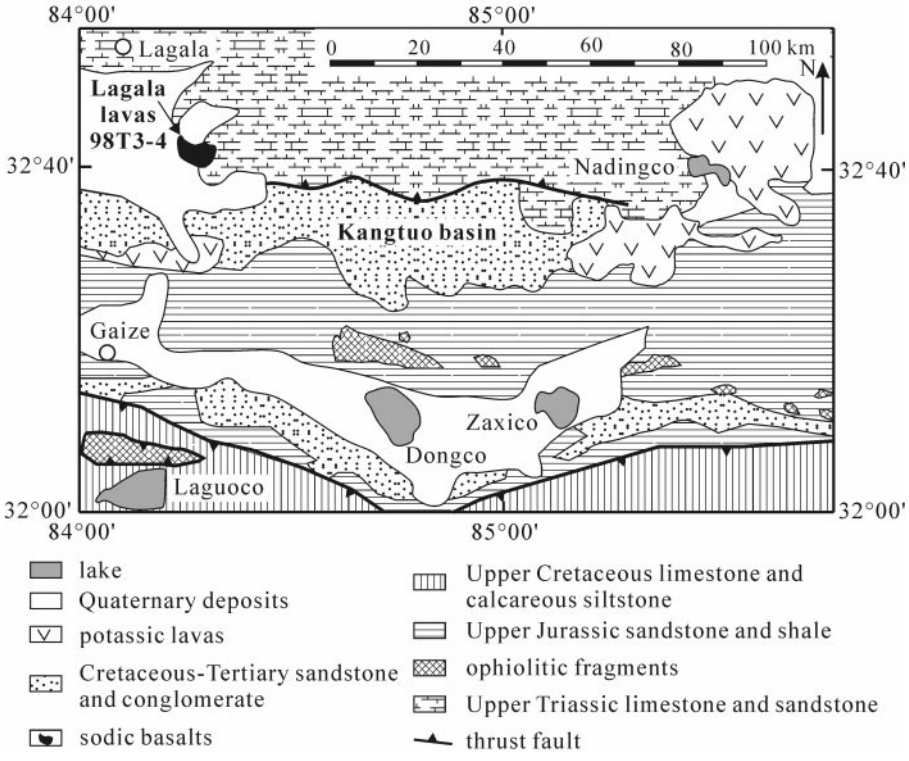

Fig. 2. Geological map of the Lagala area of the southwestern Qiangtang terrane based on Cheng & Xu (1986) and field observations during this study.

sandstone and conglomerate occur in the footwall of the north-dipping Buergahu thrust fault (Fig. 3). The non-marine sedimentary basin developed variably on top of blueschist-bearing mélange, Carboniferous sandstone and limestone, and Mesozoic sandstone.

Oligocene–Miocene potassic volcanic rocks were also discovered along the active, north-striking Wenbu–Chazi rift system of the central Lhasa terrane (Figs 1 and 4). Approximately 30 km SW of Wenbu, a horst block within the Wenbu–Chazi graben exposes a volcanic neck that intrudes early Tertiary andesite of the Linzizong Formation (Fig. 4). Just east of the town of Chazi, $\sim$300 km^2 of sheeted lavas lie on top of the eastern flank of the Wenbu–Chazi rift (Figs 1 and 4).

ANALYTICAL TECHNIQUES

Mineral separates (grain size 0·3–0·5 mm) for K–Ar and ^{40}Ar/^{39}Ar analyses were obtained using standard mineral separation techniques and hand-picked under a binocular microscope to be >99% pure. K–Ar ages (Table 1) were obtained at the Institute of Geology, China Seismological Bureau. K abundances (wt %) were determined using a HG-3 flame-photometer. Radiogenic ^{40}Ar was measured using the isotope dilution method and an MM-1200 mass spectrometer. K–Ar age calculations were made using the formulation of Dalrymple & Lanphere (1969). During the course of K–Ar analyses, repeated analyses of the internal standard, ZBH (biotite, 133·3 Ma), yielded an average age of 133·5 $\pm$ 1·5 Ma (1σ). Analytical uncertainties are estimated at $\pm$3%.

Mineral separates for ^{40}Ar/^{39}Ar analysis were irradiated for 37 h at the Beijing Nuclear Research Institute Reactor. Also irradiated were Fish Canyon sanidine (27·8 Ma; Renne *et al.*, 1994) to calculate J factors, and K_2SO_4 and CaF_2 to determine correction factors for interfering neutron reactions. All samples were step-heated using a radio-frequency furnace. Argon isotope analyses were conducted on an RGA-10 mass spectrometer in the Laboratory of Isotope Geochronology at the Institute of Geology and Geophysics, Chinese Academy of Sciences (IGCAS). Age calculations were made using the decay constants given by Steiger & Jäger (1977) and the formulations of Wang *et al.* (1985) and Wang (1992). Argon isotopic results are summarized in Table 2 and uncertainties cited in the text are at the 1σ level.

Mineral assemblages in 33 samples of Tibetan volcanic rocks, identified using a petrographic microscope, are listed in Table 3. Compositions of minerals in seven samples were determined using a CAMECA SX51 electron microprobe at the IGCAS. Multiple analyses

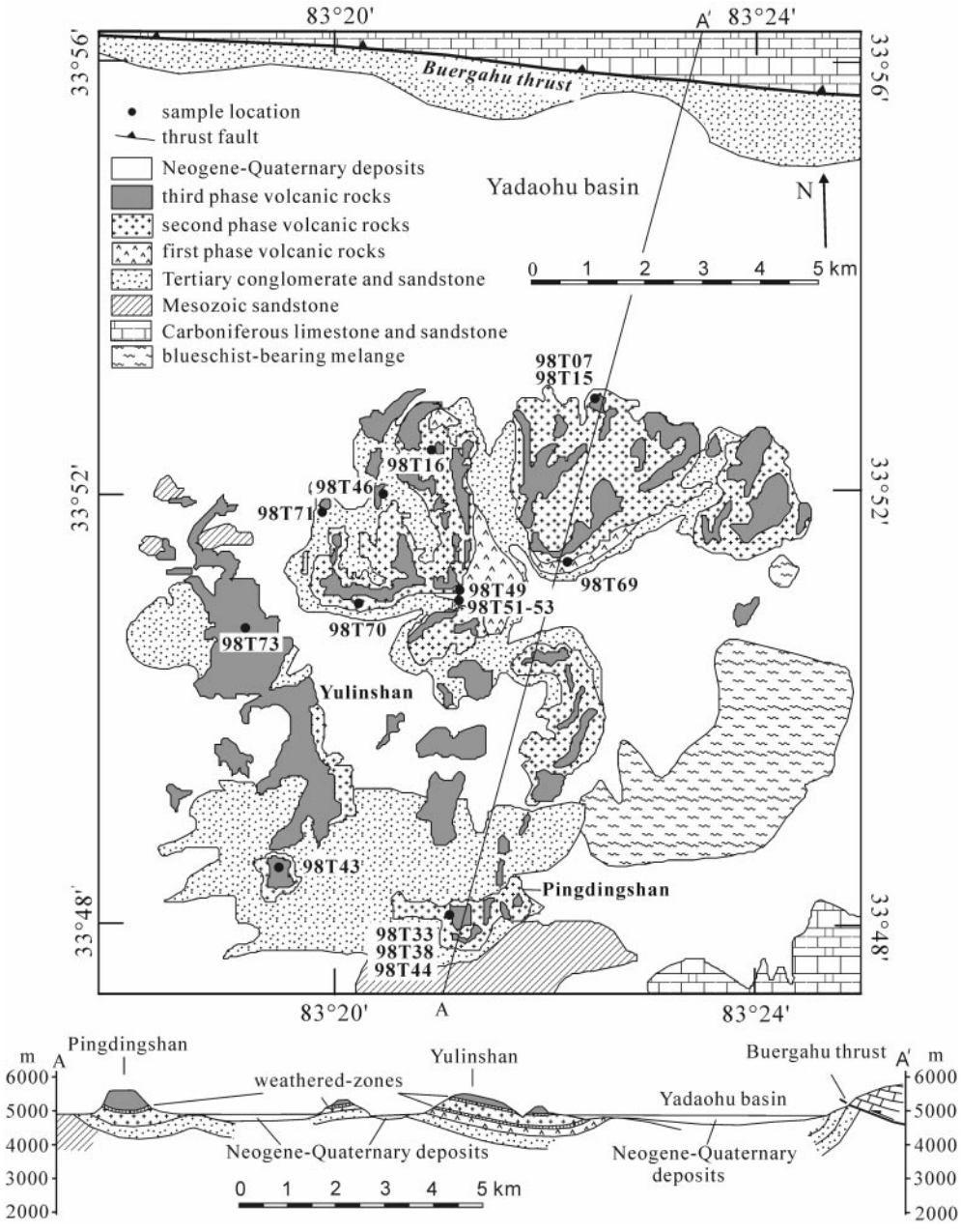

Fig. 3. Geologic map and cross-section of the Yulinshan area of the west–central Qiangtang terrane (mapping from this study).

were obtained for most of the minerals; only representative analyses are listed in Table 4. The accelerating voltage was 21 kV and the sample current was 10 nA. Beam diameters ranging from 1 to 10 μm were used, depending on the content of volatile components within the mineral being analyzed. Counting times for all elements were 10 s.

Homogeneous and unaltered rock samples were selected for chemical and isotopic analyses and results are presented in Tables 5 and 6. Five samples were selected from the Lagala ($n = 3$) and Bangdaco ($n = 2$) basaltic lavas. Eighteen samples were selected from the Yulinshan area, and include rocks from each of the three lava sheets. Five samples were selected from both the Wenbu volcanic neck and four lava sheets in the Chazi area.

For chemical analyses, hand specimens were crushed in a tungsten carbide swing mill, sieved, ultrasonically cleaned several times in deionized water and then ground in an agate mortar. Rock powders (~1·2 g) were then dissolved with $Li_2B_4O_7$ (6 g) in a TR-1000S automatic bead fusion furnace at 1100°C for

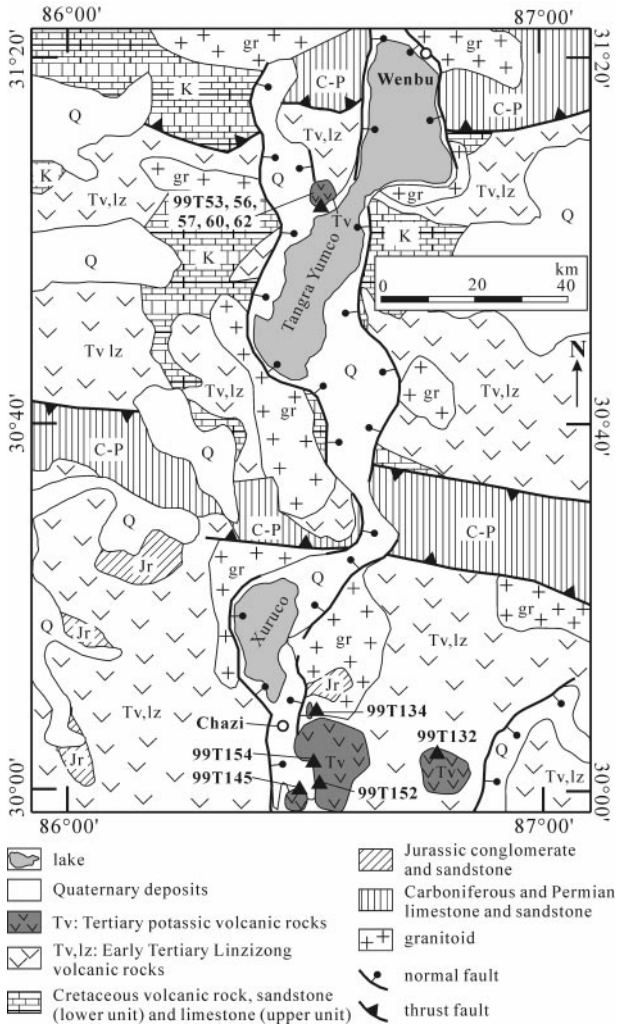

Fig. 4. Simplified geological map of the Wenbu–Chazi rift of the central Lhasa terrane based on mapping during this study and Liu (1988).

10 min. Major element abundances (wt %) were determined on whole-rock powder pellets by X-ray fluorescence (XRF) using an XRF-1500 sequential spectrometer at the IGCAS. Analytical uncertainties are 1–3% for major elements. Loss on ignition was obtained by weighing after 1 h of calcination at 1100°C. For rare earth element (REE) and trace element analyses, rock powders (50 mg) were dissolved using a mixed acid (HF:$HClO_4$ = 3:1) in capped Savillex Teflon beakers at 120°C for 6 days, and subsequently dried to wet salt and redissolved in 0·5 ml $HClO_4$. The solutions were then evaporated to wet salt at 140°C and redissolved in 1 ml HNO_3 and 3 ml water for *c.* 24 h at 120°C. The solutions were diluted in 2% HNO_3 for analysis. REE and trace element concentrations were determined by inductively coupled plasma mass spectrometry (ICP-MS) using a PQ2 Turbo

Table 1: K–Ar dating of the Yulinshan and Lagala volcanic rocks of the western Qiangtang terrane

Sample	Mineral	K (%)	^{40}Ar ($\times10^{-10}$) (mol/g)	$^{40}Ar^*$ (%)	Age ($\pm$ 1σ) (Ma)
Yulinshan					
98T44	leucite	15·95	8·553	98·34	30·66 ± 0·28
98T53	leucite	16·21	8·695	96·98	30·67 ± 0·29
98T70	leucite	14·01	7·432	97·37	30·33 ± 0·28
Lagala					
98T03	whole rock	0·52	0·543	82·75	59·18 ± 2·08

$\lambda = 5{\cdot}543 \times 10^{-10}$/a; $\lambda_e = 0{\cdot}581 \times 10^{-10}$/a; $\lambda_\beta = 4{\cdot}962 \times 10^{-10}$/a; $^{40}K/K = 1{\cdot}167 \times 10^{-4}$/mol.

system at the IGCAS. Uncertainties based on repeated analyses of internal standards are ±5% for REE and ±5–10% for trace elements.

Rb–Sr and Sm–Nd isotopic analyses were conducted on a VG354 mass spectrometer at the IGCAS. Whole-rock powders (70–50 mg) were dissolved for 7 days using a mixed acid (HF:$HClO_4$ = 3:1) in Teflon bombs, and isotopes were separated by AG50WX8 (H^+) exchangeable ion poles. Blank contributions are (2–5) $\times$ 10^{-10} g for Rb–Sr and 5 $\times$ 10^{-11} g for Sm–Nd. Within-run isotope fractionation was corrected by using $^{146}Nd/^{144}Nd = 0{\cdot}7219$ and $^{86}Sr/^{88}Sr = 0{\cdot}1194$. Eight analyses of the NBS 987 Sr standard ($^{86}Sr/^{88}Sr = 0{\cdot}710240$) yielded an average $^{86}Sr/^{88}Sr$ value of 0·710254 ± 0·000014, and 12 analyses of the La Jolla Nd standard ($^{143}Nd/^{144}Nd = 0{\cdot}511859$) yielded an average $^{143}Nd/^{144}Nd$ value of 0·511862 ± 0·000007. Depleted mantle model ages, $T(Nd)_{DM}$ were calculated using $^{147}Sm/^{144}Nd = 0{\cdot}222$ and $^{143}Nd/^{144}Nd = 0{\cdot}513114$ (Michard *et al.*, 1985). The Nd model ages probably represent minimum ages for enrichment because the Sm/Nd ratio of a melt is generally lower than that of its source. ε_{Nd} values were calculated relative to CHUR. Maximum uncertainties for $^{87}Rb/^{86}Sr$ ratios are estimated to be ±1%.

For Pb analyses, whole-rock powders (~200 mg) were dissolved for 2 weeks using a mixed acid (HF:$HClO_4$ = 10:1) in Teflon vessels. Pb was separated from the silicate matrix using AGIX8 anion exchangeable poles. Isotopic ratios were measured on a VG 354 mass spectrometer at the IGCAS. Overall blank contributions were 1–3 ng and not corrected for. Within-run Pb isotope fractionations were corrected using correction factors derived from measurements of the international standard NBS 981 ($^{206}Pb/^{204}Pb$ = 16·937,

Table 2: Summary of argon isotopic results

T (°C)	$^{40}Ar/^{39}Ar^*$	$^{37}Ar/^{39}Ar^*$	$^{36}Ar/^{39}Ar^*$ (10^{-12} mol)†	^{39}Ar (%)‡	$^{39}Ar_K \pm 1\sigma$	$^{40}Ar^*/^{39}Ar_K$§ (Ma)¶	Age $\pm 1\sigma$
98T46 sanidine (J = 0·003854, W = *0·1058 g)*							
400	341·90	0·1113	1·0440	0·000	0·01	33·50 ± 0·15	219·1 ± 40·1
500	21·260	0·2190	0·0597	0·010	0·12	3·62 ± 0·02	25·0 ± 2·7
600	7·1050	0·0487	0·0073	0·031	0·39	4·95 ± 0·04	34·1 ± 0·7
700	4·3300	0·0068	0·0041	1·030	12·79	4·20 ± 0·02	29·0 ± 0·4
800	4·3830	0·0038	0·0065	0·543	6·80	4·18 ± 0·02	28·9 ± 0·4
900	4·2630	0·0055	0·0015	1·030	12·90	4·21 ± 0·02	29·1 ± 0·4
1000	4·2960	0·0064	0·0031	1·220	15·10	4·20 ± 0·02	29·0 ± 0·4
1100	4·2270	0·0051	0·0020	2·330	29·00	4·16 ± 0·02	28·7 ± 0·4
1350	4·2340	0·0046	0·0028	1·840	22·90	4·15 ± 0·02	28·6 ± 0·4
98T69 sanidine (J = 0·003911, W = *0·0956 g)*							
500	31·070	2·9110	0·7803	0·010	0·12	8·26 ± 0·05	57·3 ± 3·7
600	5·6630	0·4320	0·0321	0·078	0·92	4·75 ± 0·03	33·2 ± 0·6
700	4·2440	0·0506	0·0025	1·040	12·16	4·17 ± 0·02	29·2 ± 0·4
800	4·2120	0·0264	0·0016	1·130	13·30	4·16 ± 0·02	29·1 ± 0·4
900	4·3490	0·0252	0·0079	0·498	5·80	4·11 ± 0·02	28·8 ± 0·4
1000	4·2840	0·0274	0·0041	0·829	9·70	4·16 ± 0·02	29·1 ± 0·4
1100	4·2920	0·0245	0·0023	1·270	14·90	4·22 ± 0·02	29·5 ± 0·4
1350	4·2750	0·0242	0·0028	3·660	43·10	4·19 ± 0·02	29·3 ± 0·4
99T60 sanidine (J = 0·008384, W = *0·118 mg)*							
360	11·871	0·0889	0·0276	0·926	0·58	3·75 ± 0·02	55·9 ± 0·8
440	8·4976	0·3498	0·0258	0·988	0·62	0·91 ± 0·01	13·6 ± 0·2
520	16·532	0·2155	0·0532	0·916	0·58	0·88 ± 0·01	13·3 ± 0·2
600	11·224	0·5470	0·0351	1·023	0·65	0·91 ± 0·01	13·7 ± 0·2
680	4·5043	0·1974	0·0122	5·335	3·37	0·90 ± 0·01	13·7 ± 0·2
800	1·4748	0·0344	0·0011	12·81	8·15	0·86 ± 0·01	13·0 ± 0·2
900	2·6896	0·0514	0·0052	6·728	4·25	1·14 ± 0·01	17·2 ± 0·2
1000	1·8095	0·0143	0·0009	19·49	12·30	1·50 ± 0·01	22·6 ± 0·3
1080	1·7952	0·0179	0·0011	19·25	12·20	1·45 ± 0·01	21·8 ± 0·3
1160	1·8524	0·0139	0·0011	14·15	8·94	1·50 ± 0·01	22·7 ± 0·3
1220	1·8253	0·0303	0·0008	38·51	24·30	1·55 ± 0·01	23·3 ± 0·3
1280	1·8554	0·0137	0·0010	19·25	12·20	1·52 ± 0·01	22·9 ± 0·3
1340	2·1691	0·0346	0·0011	12·83	8·11	1·56 ± 0·01	23·4 ± 0·3
1420	2·5294	0·0529	0·0031	5·916	3·74	1·58 ± 0·01	23·8 ± 0·3
99T62 sanidine (J = 0·008384, W = *0·112 g)*							
380	3·8085	0·0996	0·0111	2·083	0·74	0·51 ± 0·00	7·7 ± 0·1
530	8·4892	0·1823	0·0259	1·612	0·57	0·86 ± 0·01	13·0 ± 0·2
660	4·5484	0·1843	0·0124	2·157	0·77	0·89 ± 0·00	13·6 ± 0·2
780	2·1161	0·0519	0·0042	8·328	2·97	0·86 ± 0·00	13·0 ± 0·2
860	1·2947	0·0125	0·0014	22·04	7·85	0·86 ± 0·00	13·0 ± 0·2
940	1·2592	0·0124	0·0012	25·05	8·93	0·88 ± 0·01	13·2 ± 0·2
1000	1·1892	0·0097	0·0009	51·50	18·30	0·89 ± 0·01	13·5 ± 0·2
1080	1·2456	0·0098	0·0011	26·45	9·42	0·88 ± 0·02	13·3 ± 0·2
1160	2·0294	0·0241	0·0018	23·66	8·43	1·48 ± 0·03	22·3 ± 0·3
1240	2·0090	0·0152	0·0017	51·27	18·30	1·47 ± 0·02	22·2 ± 0·3

Table 2: continued

T (°C)	$^{40}Ar/^{39}Ar^*$	$^{37}Ar/^{39}Ar^*$	$^{36}Ar/^{39}Ar^*$ (10^{-12} mol)†	^{39}Ar (%)‡	$^{39}Ar_K \pm 1\sigma$	$^{40}Ar^*/^{39}Ar_K$§ (Ma)¶	Age $\pm 1\sigma$
1320	2·1542	0·0107	0·0020	43·61	15·50	1·52 ± 0·02	22·9 ± 0·3
1450	1·9188	0·0174	0·0013	22·85	8·14	1·50 ± 0·02	22·6 ± 0·3
99T132 biotite (J = 0·008384, W = *0·114 g)*							
400	6·0303	0·3585	0·0197	1·531	1·28	0·28 ± 0·01	3·6 ± 0·1
530	10·490	0·7103	0·0343	1·183	0·99	0·43 ± 0·01	6·5 ± 0·1
660	8·3750	0·8846	0·0268	1·298	1·08	0·55 ± 0·01	8·3 ± 0·2
780	2·9368	0·1517	0·0068	4·407	3·67	0·91 ± 0·01	13·7 ± 0·2
900	2·9282	0·1193	0·0069	5·173	4·31	0·87 ± 0·01	13·0 ± 0·2
1000	2·0354	0·0340	0·0038	13·11	10·90	0·89 ± 0·02	13·4 ± 0·2
1080	1·7991	0·0375	0·0031	15·08	10·90	0·87 ± 0·02	13·1 ± 0·2
1160	1·9602	0·0239	0·0035	40·83	34·00	0·90 ± 0·01	13·5 ± 0·2
1260	2·3656	0·0509	0·0030	10·79	8·99	1·46 ± 0·03	21·9 ± 0·3
1360	4·2408	0·0590	0·0092	17·72	14·80	1·52 ± 0·03	22·9 ± 0·3
1450	6·3158	0·0895	0·0163	8·815	7·35	1·50 ± 0·04	22·5 ± 0·3

*Corrected for backgrounds, mass discrimination, abundance sensitivity and radioactive decay.
†Normalized to 100% delivery to mass spectrometer.
‡Includes contribution from static line blank.
§Corrected for atmospheric argon and nucleogenic interferences.
¶Assumes trapped argon is atmospheric.
J, irradiation parameter; *W*, weight of sample; *T*, temperature. The sensitivity of the mass spectrometer was $8{\cdot}4 \times 10^{-3}$ A/Pa (corresponding to $1{\cdot}42 \times 10^{-14}$ mol/mV) and the static vacuum was *c*. 3×10^{-6} Pa. Typical background values for ^{40}Ar, ^{39}Ar, ^{37}Ar and ^{36}Ar were $2{\cdot}44 \times 10^{-14}$, $5{\cdot}82 \times 10^{-16}$, $4{\cdot}61 \times 10^{-16}$ and $5{\cdot}43 \times 10^{-16}$ mol, respectively, and were measured before each sample analysis. Correction factors: $(^{36}Ar/^{37}Ar)_{Ca} = 2{\cdot}64 \times 10^{-4}$, $(^{40}Ar/^{39}Ar)_K = 3{\cdot}05 \times 10^{-2}$, $(^{39}Ar/^{37}Ar)_{Ca} = 6{\cdot}87 \times 10^{-4}$. Measured $^{40}Ar/^{36}Ar_{atm} = 294{\cdot}1$.

$^{207}Pb/^{204}Pb = 15{\cdot}491$ and $^{208}Pb/^{204}Pb = 36{\cdot}721$; Catanzaro *et al*., 1968). Five analyses of the NBS 981 Pb standard yielded $^{206}Pb/^{204}Pb = 16{\cdot}927 \pm 0{\cdot}014$, $^{207}Pb/^{204}Pb = 15{\cdot}476 \pm 0{\cdot}015$ and $^{208}Pb/^{204}Pb = 36{\cdot}624 \pm 0{\cdot}042$. Calculated mass fractionation was ~0·2% per atomic mass unit.

GEOCHRONOLOGY

A sample of Lagala basalt (98T03) yielded a whole-rock K–Ar age of 59·2 ± 2·1 Ma (Table 1). This age should be considered tentative until additional data become available, but is reasonable considering that volcanic rocks of similar age and lithology occur ~400 km to the NW in the Aksayqin area (60–45 Ma; Deng, 1998) and <45 km to the north (total gas $^{40}Ar/^{39}Ar$ age of 65·0 ± 0·7 Ma) and south ($^{40}Ar/^{39}Ar$ plateau age of 64·4 ± 0·7 Ma) of the Lagala area (Kapp *et al*., 2002) (Fig. 1).

K–Ar analyses of leucite phenocrysts from three samples of Yulinshan leucite phonolites (98T44, 98T53 and 98T70) yield apparent ages of 30·3 ± 0·3, 30·7 ± 0·3 and 30·7 ± 0·3 Ma (Table 1). It is unlikely that the three samples were affected by excess argon or argon loss as a result of alteration, as they yield consistent K–Ar ages and a linear correlation on a K–Ar isochron diagram (isochron age of 30·8 ± 0·6 Ma). $^{40}Ar/^{39}Ar$ analyses of sanidine phenocrysts from two samples of Yulinshan trachytes (98T46 and 98T69) yield two well-defined plateau ages of 28·9 ± 0·4 and 29·2 ± 0·4 Ma (Table 2 and Fig. 5). From the above results, it is concluded that Yulinshan volcanism was active during the time interval of 31–29 Ma.

$^{40}Ar/^{39}Ar$ analyses were conducted on sanidine phenocrysts from two samples from the Wenbu volcanic neck (99T60 and 99T62; Table 2 and Fig. 5). Sample 99T60 yields a plateau age of 13·4 ± 0·5 Ma during the initial 14% ^{39}Ar released and an older, slightly monotonically increasing plateau with a weighted mean $^{40}Ar/^{39}Ar$ age of 22·9 ± 0·7 Ma (increments 8–14; 82% of ^{39}Ar released). Sample 99T62 also yields two distinct $^{40}Ar/^{39}Ar$ age plateaux; a younger plateau at 13·2 ± 0·4 Ma (increments 2–8; 49% of ^{39}Ar released) and an older plateau at 22·5 ± 0·5 Ma (increments 9–12; 50% of ^{39}Ar released). For the two samples, the older plateau ages of ~23 Ma are interpreted to be the

Table 3: Phenocryst and groundmass mineralogy of Cenozoic volcanic rocks from the western Qiangtang and central Lhasa terranes

Sample no.	Lithology	Texture	Phenocrysts	Groundmass
Lagala				
98T03	alkali basalt	vitrophyric	Ol	Cpx + Ol + Pl + Ti-Mt + Ap + glass
98T04	alkali basalt	vitrophyric	Ol	Cpx + Ol + Pl + Ti-Mt + Ap + glass
Bangdaco				
02T394	hawaiite	vitrophyric	Ol	Cpx + Ol + Pl + Ti-Mt + Ap + glass
02T395	hawaiite	vitrophyric	Ol	Cpx + Ol + Pl + Ti-Mt + Ap + glass
02T396	hawaiite	vitrophyric	Ol	Cpx + Ol + Pl + Ti-Mt + Ap + glass
Yulinshan				
98T52	basaltic trachyandesite	porphyritic	Cpx + Sa + No + Ha + Ne + Bi	Cpx + Sa + No + Ha + Ne + Phl + Ap + Ti-Mt + glass
98T15	trachyandesite	porphyritic	Cpx + Sa + No + Ne + Sph	Cpx + Sa + No + Ha + Ne + Ap + Ti-Mt + glass
98T33	trachyandesite	porphyritic	Cpx + Sa + No	Cpx + Sa + No + Ha + Ne + Ap + Ti-Mt + glass
98T49	trachyandesite	porphyritic	Cpx + Sa	Cpx + Sa + No + Ap + Ti-Mt
98T51	trachyandesite	porphyritic	Cpx + Sa + No + Ha	Cpx + Sa + No + Ha + Ne + Ti-Mt + Ap
98T73	trachyandesite	porphyritic	Cpx + Sa + No + Ha + Ne	Cpx + Sa + No + Ha + Ne + Ap + glass
98T07	tephriphonolite	porphyritic	Cpx + Sa + Lc + No + Ne + Bi	Cpx + Sa + Lc + Ne + No + Ha + Sph + Ap + Ti-Mt
98T57	tephriphonolite	porphyritic	Cpx + Sa + Lc + No + Ne	Cpx + Sa + Lc + Ne + No + Ha + Sph + Ap
98T44	tephriphonolite	porphyritic	Cpx + Sa + Lc + No + Ne + Sph	Cpx + Sa + Lc + Ne + No + Sph + Ap
98T53	tephriphonolite	porphyritic	Cpx + Sa + Lc + No + Ne	Cpx + Sa + Lc + Ne + No + Ap + Ti-Mt
98T54	tephriphonolite	porphyritic	Cpx + Sa + Lc + No + Ne	Cpx + Sa + Lc + Ne + No + Ap + Ti-Mt
98T69	tephriphonolite	porphyritic	Cpx + Sa + Lc + No + Ne	Cpx + Sa + Lc + Ne + Ap
98T70	tephriphonolite	porphyritic	Cpx + Sa + Lc + No + Ne	Cpx + Sa + Lc + Ne + No + Ha + Ap + Ti-Mt
98T16	trachyte	trachytic	Ae + Sa	Ae + Sa + So + Ne + Mag + Ti-Mt
98T38	trachyte	trachytic	Sa	Ae + Sa + So + Ne + Ti-Mt
98T43	trachyte	trachytic		Ae + Sa + So + Ne + Sph + Ap + Ti-Mt
98T46	trachyte	trachytic	Sa	Ae + Sa + So + Ne + Ti-Mt + glass
98T71	trachyte	trachytic		Ae + Sa + Ne + Sph + Ap + Ti-Mt
Wenbu				
99T53	trachyte	porphyritic	Phl + Cpx + Sa	Phl + Cpx + Sa + Ap + Ti-Mt
99T57	trachyte	porphyritic	Phl + Cpx + Sa + Lc	Phl + Cpx + Sa + Lc + Ap + Ti-Mt
99T56	phonolite	porphyritic	Phl + Cpx + Sa	Phl + Cpx + Sa + Ap + Ti-Mt
99T60	phonolite	porphyritic	Phl + Cpx + Sa	Phl + Cpx + Sa + Ap + Ti-Mt
99T62	trachyte	porphyritic	Phl + Cpx + Sa + Lc	Phl + Cpx + Sa + Lc + Ap + Ti-Mt
Chazi				
99T132	phonotephrite	porphyritic	Phl + Cpx	Phl + Cpx + Sa + Lc + Ap + Ti-Mt + glass
99T134	trachyte	porphyritic	Phl + Sa	Phl + Sa + Ap + Ti-Mt + glass
99T145	trachyte	porphyritic	Phl + Sa	Phl + Sa + Ap + Ti-Mt + glass
99T152	trachyte	porphyritic	Phl + Cpx + Sa	Phl + Cpx + Sa + Ap + Ti-Mt + glass
99T154	trachyandesite	porphyritic	Phl + Cpx + Sa	Phl + Cpx + Sa + Ap + Ti-Mt + glass

Ae, aegirine; Ap, apatite; Bi, biotite; Cpx, clinopyroxene; Ha, haüyne; Lc, leucite; Mag, magnesioriebeckite; Ne, nepheline; No, nosean; Ol, olivine; Pl, plagioclase; Sa, sanidine; So, sodalite; Sph, sphene; Ti-Mt, Ti-magnetite.

best estimate for the age of volcanism. The younger plateau ages at ~13 Ma are interpreted to represent the time when the volcanic neck was cooled to below the closure temperature for Ar in the smallest sanidine crystals. This interpretation is consistent with the presence of 25–17 Ma volcanic rocks in the western Lhasa terrane (Miller *et al.*, 1999) and extension-related denudation in Tibet at ~13 Ma (Coleman &

Table 4: Representative electron microprobe analyses of minerals in Cenozoic volcanic rocks from the western Qiangtang and central Lhasa terranes

Mineral	SiO_2	TiO_2	Al_2O_3	Cr_2O_3	FeO	Fe_2O_3	MgO	CaO	MnO	NiO	Na_2O	K_2O	BaO	H_2O	SO_2	Cl	Total
Lagala, sample 98T03, basalt																	
Ol (3)	38·81	0·00	0·03	0·06	18·63	—	41·56	0·38	0·55	0·10	0·00	0·03	—	—	—	—	100·03
Cpx (9)	49·26	1·44	4·57	0·00	4·30	3·08	13·96	21·71	0·14	0·00	0·66	0·00	—	—	—	—	99·13
Pl (3)	54·58	0·12	27·65	0·00	0·79	—	0·06	10·70	0·04	0·00	5·25	0·24	—	—	—	—	99·42
Bangdaco, sample 02T194, basalt																	
Ol (5)	39·12	0·03	0·04	0·02	15·15	—	45·03	0·23	0·21	0·05	0·03	0·00	—	—	—	—	99·91
Cpx (6)	45·25	2·31	9·12	0·30	5·78	—	12·95	23·15	0·10	0·01	0·60	0·02	—	—	—	—	99·59
Pl (2)	55·28	0·20	27·22	0·00	0·47	—	0·08	10·56	0·03	0·00	5·18	0·51	—	—	—	—	99·53
Yulinshan, sample 98T52, basaltic trachyandesite																	
Cpx (5)	48·05	0·94	2·68	0·00	12·59	5·71	7·39	20·16	0·55	0·00	1·69	0·03	—	—	—	—	99·79
Sa (2)	65·25	0·09	18·26	0·00	0·22	—	0·00	0·19	0·01	0·00	3·23	12·25	—	—	—	—	99·49
Bi (3)	35·04	8·83	13·85	0·02	13·06	—	13·79	0·00	0·12	0·04	0·50	7·97	2·11	4·30	—	—	99·58
Ne (2)	47·60	0·07	28·13	0·00	2·14	—	0·04	0·10	0·00	0·00	16·27	5·38	—	—	—	—	99·73
No (1)	38·30	0·00	28·58	0·00	0·73	—	0·02	0·60	0·00	0·03	16·54	3·77	—	—	8·04	3·01	99·62
Yulinshan, sample 98T53, tephriphonolite																	
Cpx (3)	49·89	1·23	3·01	0·00	6·26	5·26	11·29	22·05	0·27	0·00	1·26	0·00	—	—	—	—	100·52
Sa (3)	64·90	0·13	18·77	0·01	0·72	—	0·02	0·13	0·00	0·00	3·40	11·00	—	—	—	—	99·09
Lc (7)	55·70	0·02	21·15	0·01	0·91	—	0·00	0·00	0·00	0·00	0·04	21·50	—	—	—	—	99·33
Ne (1)	44·92	0·03	31·24	0·03	1·89	—	0·04	0·06	0·00	0·00	16·64	5·70	—	—	—	—	100·53
Ha (4)	37·94	0·00	29·61	0·05	0·64	—	0·01	1·20	0·00	0·05	15·68	4·46	—	—	9·58	—	99·21
No (2)	38·30	0·00	28·58	0·00	0·73	—	0·02	0·60	0·00	0·03	16·54	3·77	—	—	8·04	3·31	99·92
Yulinshan, sample 98T38, trachyte																	
Ae (5)	51·56	0·38	2·03	0·03	7·17	24·40	0·18	2·24	0·27	0·06	11·44	0·09	—	—	—	—	99·85
Sa (2)	65·25	0·09	18·26	0·00	0·22	—	0·00	0·19	0·01	0·00	3·23	12·25	—	—	—	—	99·49
So (6)	39·55	0·00	29·56	0·01	1·67	—	0·01	0·00	0·02	0·00	25·42	0·10	—	—	0·46	3·12	99·91
Wenbu, sample 99T63, tephriphonolite																	
Cpx (2)	53·82	0·45	0·33	0·09	3·89	1·24	16·60	23·03	0·14	0·04	0·34	0·01	—	—	—	—	99·96
Sa (1)	63·33	0·10	17·72	0·00	0·65	—	0·01	0·00	0·00	—	0·88	14·91	1·30	—	—	—	98·92
Phl (4)	39·16	5·57	11·09	0·07	9·83	—	19·81	0·02	0·09	0·11	0·38	9·67	—	4·11	—	—	99·90
Chazi, sample 99T132, tephriphonolite																	
Cpx (2)	52·85	0·31	1·30	0·03	3·02	2·42	16·57	22·82	0·11	0·02	0·34	0·00	—	—	—	—	99·77
Sa (1)	54·39	0·05	20·68	0·01	0·95	—	0·02	0·00	0·00	—	0·16	20·78	0·00	—	—	—	97·04
Lc (2)	55·64	0·08	21·30	0·05	0·93	—	0·02	0·00	0·02	—	0·15	19·39	0·00	—	—	—	97·57
Phl (3)	39·81	2·52	12·58	0·14	8·50	—	22·50	0·11	0·07	0·05	0·32	9·61	—	3·17	—	—	99·37

Ae, aegirine; Bi, biotite; Cpx, clinopyroxene; Ha, haüyne; Lc, leucite; Ne, nepheline; No, nosean; Ol, olivine; Pl, plagioclase; Phl, phlogopite; Sa, sanidine; So, sodalite. Number in parentheses indicates total number of analyses that were determined for each mineral; if more than one, only representative analyses are listed.

Hodges, 1995; Blisniuk *et al.*, 2001; Williams *et al.*, 2001). However, additional $^{40}Ar/^{39}Ar$ analyses on sanidine separates of variable sizes are needed to test this interpretation.

Sanidine and phlogopite phenocrysts from two samples of lavas from the Chazi area (99T132 and 99T154) yield similar $^{40}Ar/^{39}Ar$ plateau ages of 13·3 ± 0·4 Ma (increments 4–8; 64% of ^{39}Ar released) and 13·1 ± 0·3 Ma (increments 6–11; 87% of ^{39}Ar released), respectively (Fig. 5). Sanidine phenocrysts from a sample of a volcanic cone (99T145) within the Chazi graben yield a younger $^{40}Ar/^{39}Ar$ plateau age of

Table 5: Major (wt %) and trace element (ppm) concentrations for Cenozoic volcanic rocks from the western Qiangtang and central Lhasa terranes

Location:	Lagala		Bangdaco			Yulinshan											
Sample:	98T03	98T04	2T394	2T395	2T396	98T07	98T15	98T16	98T33	98T38	98T43	98T44	98T46	98T49	98T51	98T52	98T53
SiO_2	48·41	47·20	44·98	44·30	44·91	53·84	51·20	55·91	51·83	57·62	56·94	47·78	56·46	54·00	53·87	47·37	51·27
TiO_2	1·17	1·78	2·15	2·15	2·30	1·10	1·17	0·79	1·15	0·82	0·87	1·04	0·80	0·97	0·71	1·13	0·90
Al_2O_3	15·21	15·13	15·99	16·05	15·88	17·41	15·53	13·24	16·78	13·56	13·32	17·50	14·72	18·18	14·85	14·40	16·75
Fe_2O_3	9·50	9·91	11·79	11·70	11·86	6·27	7·65	9·38	7·85	9·04	8·93	7·25	8·00	5·95	7·55	6·70	7·17
MnO	0·17	0·15	0·18	0·19	0·16	0·17	0·20	0·25	0·21	0·27	0·25	0·19	0·32	0·17	0·26	0·12	0·21
MgO	9·48	8·80	7·01	7·30	7·02	1·02	2·49	0·89	0·73	0·48	0·48	1·06	0·69	0·71	0·72	3·68	0·97
CaO	10·07	9·32	7·99	8·40	8·13	4·04	5·95	3·93	3·50	3·78	4·28	5·29	3·25	3·71	5·46	9·69	4·94
Na_2O	3·53	3·76	4·60	4·50	4·58	3·89	3·01	3·85	2·52	4·74	4·32	2·58	3·39	3·28	3·60	2·97	4·17
K_2O	0·50	0·67	0·98	1·20	0·94	7·68	4·89	5·91	6·66	5·83	5·83	8·51	6·36	6·83	6·57	3·21	8·07
P_2O_5	0·41	0·52	0·80	0·65	0·85	0·17	0·41	0·03	0·09	0·05	0·13	0·23	0·01	0·02	0·29	1·02	0·17
LOI	1·76	2·46	2·97	3·20	2·91	3·84	5·61	4·80	7·09	3·40	3·74	5·74	4·35	5·68	5·93	6·49	4·17
Total	100·21	99·70	99·44	99·60	99·54	99·43	98·11	98·98	98·41	99·59	99·09	97·17	98·35	99·50	99·81	96·97	98·79
mg-no.	66·41	63·77	54·10	55·29	53·97	24·38	39·21	15·83	15·57	9·52	9·63	22·47	14·59	19·11	15·89	46·59	21·15
La	33	37	66	65	64	536	359	683	491	755	649	760	639	403	553	387	322
Ce	71	80	121	120	118	927	672	1134	852	1221	1123	1190	1068	697	934	707	578
Pr	8·2	9·0	12·9	12·4	12·2	90·0	66·7	112·6	79·3	126·8	115·8	99·8	107·2	63·3	89·7	70·1	54·6
Nd	31	34	48	46	46	270	211	303	253	341	310	310	268	189	247	229	169
Sm	6·3	7·1	8·1	7·9	8·1	36·5	30·1	39·5	35·2	44·1	40·9	53·2	33·7	24·0	30·8	31·4	22·7
Eu	1·9	2·1	3·0	2·8	2·8	9·0	7·3	9·4	8·3	10·4	9·5	12·4	7·8	5·4	6·9	6·8	5·3
Gd	6·1	6·5	7·3	7·0	7·2	25·8	20·4	26·0	19·4	28·1	26·0	33·0	20·0	15·9	21·5	20·4	14·6
Tb	1·0	1·0	1·1	1·0	1·1	3·4	2·7	3·5	2·7	4·0	3·6	4·1	3·0	2·0	2·7	2·5	1·9
Dy	5·6	5·9	5·6	5·0	5·4	15·5	12·1	16·0	12·3	17·7	16·1	18·9	13·9	8·9	11·9	10·4	8·3
Ho	1·1	1·2	1·1	1·0	1·0	2·7	2·1	2·8	1·9	3·2	2·9	2·7	2·3	1·4	2·1	1·6	1·3
Er	3·1	3·3	2·8	2·5	2·7	7·4	5·2	7·3	5·0	8·3	7·3	7·7	6·4	3·9	5·7	4·2	3·5
Tm	0·4	0·5	0·4	0·4	0·4	1·0	0·7	1·0	0·7	1·2	1·0	1·1	1·0	0·6	0·8	0·6	0·5
Yb	2·9	3·2	2·3	2·1	2·4	6·0	4·4	6·3	4·5	7·1	6·3	6·8	6·1	3·6	5·0	3·5	3·1
Lu	0·4	0·5	0·4	0·3	0·4	0·9	0·6	0·9	0·7	1·1	0·9	1·0	0·9	0·5	0·8	0·5	0·5
Sc	29·9	33·0	—	—	—	9·4	8·0	5·4	3·7	5·7	6·8	7·6	3·3	5·3	4·7	9·1	4·4
Cr	768	839	209	204	215	44	61	19	16	20	18	32	22	56	21	30	17
Co	49	49	34	38	35	6·3	11·4	1·9	3·6	3·1	3·1	12·6	2·2	3·8	2·8	15·9	3·0
Ni	218	189	97	95	94	7·9	25·1	1·1	1·1	1·8	1·4	5·0	1·1	2·6	2·2	11·7	1·9
Cu	69	66	41	45	41	9·1	11·8	5·1	1·3	4·5	2·3	11·0	8·5	3·7	2·5	18·9	3·0
Zn	89	83	95	100	99	279	226	313	201	326	299	309	264	144	225	140	121
Rb	10	11	9·0	8·8	8·6	138	97	137	146	137	114	181	122	236	161	317	132
Sr	741	950	1162	1138	1122	8102	8843	12239	8614	6849	7309	15881	11258	7998	5409	11985	5150
Y	31	35	26	25	25	82	60	86	57	95	82	89	76	45	62	50	42
Zr	170	204	259	253	250	1178	785	1103	726	1205	1052	1064	1098	653	853	555	542
Nb	15	18	65	66	61	154	59	101	89	116	104	92	97	73	81	42	63
Cs	39	46	1·7	1·7	1·6	3·4	1·6	2·0	1·6	4·0	1·6	3·3	2·6	3·0	8·9	3·7	2·2
Ba	300	391	929	911	894	3579	6903	1651	4553	1573	2102	15973	3354	6267	2448	7609	3914
Hf	5·3	6·4	5·9	5·5	5·6	30	18	27	16	30	26	25	27	15	22	12	11
Ta	0·8	1·3	4·5	4·2	3·9	6·2	3·5	2·8	4·0	3·4	3·3	6·3	3·2	3·3	2·6	3·2	2·7
Pb	8·6	8·4	7·5	6·9	7·2	207	134	316	144	339	282	201	276	117	249	81	95
Th	4·7	5·5	8·9	8·3	8·3	191	69	195	134	219	194	62	178	59	148	52	48
U	1·2	1·5	2·2	2·0	2·1	19	6·7	18	7·1	21	23	11	12	5·8	10	5·8	7·8

Table 5: continued

Location:	Yulinshan						Wenbu					Chazi				
Sample:	98T54	98T57	98T69	98T70	98T71	98T73	99T53	99T56	99T57	99T60	99T62	9T132	9T134	9T145	9T152	9T154
SiO_2	54·09	51·02	50·54	48·68	56·26	52·91	60·15	59·45	56·79	59·22	58·90	49·71	68·54	65·02	60·45	56·81
TiO_2	0·33	0·92	1·01	1·06	0·82	0·72	1·24	1·22	1·43	1·26	1·26	1·08	0·66	0·66	0·98	0·97
Al_2O_3	20·44	16·31	17·58	16·77	14·20	15·81	14·47	13·91	13·29	14·02	13·93	11·85	14·07	14·67	13·71	12·71
Fe_2O_3	2·67	7·57	7·04	6·91	7·50	7·20	3·76	4·19	5·07	4·16	4·16	7·49	3·15	3·387	4·82	5·58
MnO	0·34	0·22	0·19	0·17	0·25	0·21	0·12	0·13	0·16	0·13	0·16	0·24	0·14	0·16	0·17	0·19
MgO	0·60	0·65	0·95	1·15	0·76	0·16	2·06	3·07	3·24	3·36	3·51	7·18	1·11	1·5	3·82	4·59
CaO	2·63	4·81	4·92	6·52	2·65	5·59	2·79	3·04	3·70	2·95	3·92	10·34	1·24	2·26	4·86	7·12
Na_2O	3·46	3·68	2·89	2·16	4·46	2·60	1·92	2·24	2·34	1·26	1·96	1·62	2·68	2·57	2·41	1·80
K_2O	9·38	6·58	7·96	7·36	6·02	6·98	10·55	11·24	8·62	11·66	10·09	6·17	6·54	7·38	7·53	8·19
P_2O_5	0·93	0·11	0·12	0·12	0·36	0·02	0·57	0·47	0·56	0·46	0·67	1·34	0·37	0·43	0·59	0·77
LOI	4·31	6·04	5·25	7·06	4·55	6·40	1·78	1·06	4·18	1·18	1·01	2·63	1·21	1·76	0·67	1·16
Total	99·18	97·91	98·45	97·96	97·83	98·60	99·41	100·0	99·38	99·66	99·57	99·65	99·71	99·8	100·0	99·89
mg-no.	5·00	14·54	21·10	24·81	16·72	4·22	52·02	59·23	55·86	61·54	62·56	65·50	41·10	46·74	61·10	61·98
La	237	538	400	356	574	590	232	288	292	254	247	142	97	111	110	116
Ce	474	955	725	622	967	996	486	560	591	514	507	314	198	229	250	252
Pr	48	75	68	59	96	100	56	69	68	57	58	39	20	25	30	32
Nd	158	257	209	184	253	259	203	253	246	207	213	156	77	95	118	131
Sm	21	34	28	25	34	33	29	31	38	26	29	31	11	17	22	25
Eu	4·4	7·7	6·2	5·2	7·5	7·7	5·8	6·7	7·9	5·0	5·6	7·1	2·7	3·5	4·2	4·9
Gd	12	19	19	17	22	22	17	21	24	17	19	22	5·6	9·8	11	14
Tb	1·4	2·9	2·4	2·0	2·8	2·8	1·7	2·0	2·2	1·8	1·8	2·5	0·9	1·4	1·5	1·9
Dy	5·8	13	10	8·6	12	13	5·5	5·3	6·9	4·9	5·2	9·8	3·5	5·0	5·9	6·4
Ho	0·8	2·0	1·6	1·3	2·2	2·3	0·8	0·8	1·2	0·7	0·8	1·5	0·5	0·8	0·9	1·0
Er	2·3	5·6	4·3	3·6	5·7	6·0	2·7	2·8	3·5	2·0	2·4	3·8	1·4	2·0	2·3	2·8
Tm	0·3	0·8	0·6	0·5	0·8	0·8	0·2	0·3	0·4	0·2	0·3	0·4	0·2	0·2	0·3	0·3
Yb	1·5	5·0	3·7	3·2	5·2	5·3	1·7	1·8	2·1	1·2	1·7	2·3	1·0	1·4	1·6	1·7
Lu	0·2	0·7	0·5	0·5	0·8	0·8	0·2	0·2	0·3	0·2	0·2	0·3	0·1	0·2	0·2	0·2
Sc	4·0	4·5	6·0	5·8	5·4	7·3	—	—	—	—	—	—	—	—	—	—
Cr	25	17	19	20	25	26	124	129	139	181	134	123	114	68	154	131
Co	0·2	3·1	5·5	7·8	3·3	2·9	13	13	15	15	17	30	9·2	9·5	19	22
Ni	0·7	1·9	1·6	3·1	4·4	2·7	68	74	67	102	103	117	45	44	100	101
Cu	3·4	1·4	3·8	9·7	2·4	3·3	26	23	62	32	32	65	22	29	40	54
Zn	88	251	187	134	238	237	6·5	7·3	10·1	6·0	7·4	7·0	5·4	7·1	4·8	7·7
Rb	401	101	146	605	133	230	372	455	353	432	416	676	479	506	586	619
Sr	5619	15352	8933	9166	5889	7592	1377	1077	1760	1028	1907	1490	552	745	843	1556
Y	25	66	50	42	62	67	20	23	30	18	22	40	14	22	23	27
Zr	113	882	624	552	1011	926	1154	929	1534	786	679	511	197	271	352	428
Nb	18	69	53	62	97	85	73	50	106	43	53	25	23	28	29	24
Cs	11	1·9	2·1	3·4	2·1	3·6	14	6·8	26	14	6·2	33	17	21	33	30
Ba	4264	3421	8175	7934	3466	2070	3648	3574	5160	3167	3035	3209	1256	1594	1757	2108
Hf	2·4	19	13	12	25	22	30	26	40	24	19	13	6·3	8·5	9·7	11·4
Ta	0·5	4·0	3·6	3·0	3·5	2·8	4·3	5·2	5·2	3·7	3·3	1·6	1·6	2·4	2·1	1·9
Pb	12	167	113	95	173	235	167	116	201	87	92	93	62	54	55	113
Th	34	96	57	50	160	157	214	223	283	160	176	129	108	145	117	116
U	1·7	15	9·3	11	11	19	23	12	43	5·2	4·8	18	17	21	25	8·4

mg-number = 100 × [Mg/(Mg + Fe_{total})].

Table 6: Sr, Nd and Pb isotopic data for Cenozoic volcanic rocks from the western Qiangtang and central Lhasa terranes

Sample	Age (Ma)	Rb (ppm)	Sr (ppm)	$^{87}Rb/^{86}Sr$	$^{87}Sr/^{86}Sr$ ±2σ	$^{87}Sr/^{86}Sr(i)$	Sm (ppm)	Nd (ppm)	$^{147}Sm/^{144}Nd$	$^{143}Nd/^{144}Nd$ ±2σ	ε(t)Nd	$T(Nd)_{DM}$ (Ga)	$T(Nd)_{CHUR}$ (Ga)	$^{206}Pb/^{204}Pb$ ±2σ	$^{207}Pb/^{204}Pb$ ±2σ	$^{208}Pb/^{204}Pb$ ±2σ
Lagala																
98T03	60				0·70593 ± 2					0·512438 ± 9	−3·90			18·888 ± 3	15·605 ± 3	38·891 ± 6
98T04	60				0·70606 ± 2					0·512461 ± 5	−3·45			18·813 ± 3	15·556 ± 5	38·962 ± 2
Bangdaco																
02T394	60–45	16·6	1120	0·0432	0·70464 ± 2	0·704615	7·9	49·2	0·105976	0·512657 ± 13	−0·24	0·64	0·02	18·214 ± 2	15·501 ± 2	38·420 ± 2
02T395	60–45	16·7	1111	0·0435	0·70471 ± 1	0·704687	7·7	46·5	0·105321	0·512711 ± 23	0·82	0·57	—	18·414 ± 2	15·513 ± 2	38·620 ± 2
02T396	60–45	16·8	1104	0·0439	0·70460 ± 2	0·704573	7·8	47·2	0·105942	0·512658 ± 10	−0·22	0·64	0·02	18·387 ± 1	15·490 ± 2	38·563 ± 1
98T07	30				0·70903 ± 2					0·512213 ± 6	−8·29			18·964 ± 3	15·702 ± 4	39·315 ± 7
98T15	30	112	8968	0·0373	0·70903 ± 2	0·709012	29·8	209·8	0·08800	0·512228 ± 6	−8·00	1·03	0·60	19·105 ± 2	15·828 ± 6	39·687 ± 2
98T16	30				0·70916 ± 2					0·512195 ± 7	−8·64			19·012 ± 1	15·731 ± 3	39·411 ± 1
98T33	30				0·70906 ± 2					0·512218 ± 7	−8·19			18·883 ± 4	15·642 ± 4	39·139 ± 9
98T38	30				0·70921 ± 2					0·512166 ± 6	−9·21			19·052 ± 1	15·766 ± 4	39·557 ± 1
98T43	30				0·70910 ± 1					0·512192 ± 9	−8·70			18·984 ± 3	15·696 ± 4	39·325 ± 5
98T44	30				0·70906 ± 2					0·512187 ± 7	−8·80			18·936 ± 3	15·675 ± 4	39·239 ± 8
98T46	30				0·70906 ± 2					0·512206 ± 6	−8·43			19·058 ± 3	15·761 ± 3	39·510 ± 1
Yulinshan																
98T49	30				0·70883 ± 1					0·512197 ± 8	−8·60			18·946 ± 4	15·676 ± 4	39·274 ± 8
98T51	30				0·70896 ± 2					0·512205 ± 9	−8·45			18·967 ± 2	15·704 ± 4	39·343 ± 7
98T52	30				0·70898 ± 1					0·512233 ± 5	−7·90			18·966 ± 5	15·699 ± 5	39·346 ± 9
98T53	30				0·70901 ± 2					0·512232 ± 8	−7·92			18·944 ± 4	15·667 ± 4	39·211 ± 8
98T54	30				0·70905 ± 3					0·512215 ± 10	−8·25			18·987 ± 2	15·730 ± 4	39·427 ± 7
98T57	30				0·70911 ± 2					0·512172 ± 7	−9·09			19·026 ± 2	15·744 ± 3	39·437 ± 6

Table 6: continued

Sample	Age (Ma)	Rb (ppm)	Sr (ppm)	$^{87}Rb/^{86}Sr$	$^{87}Sr/^{86}Sr$ ±2σ	$^{87}Sr/^{86}Sr(i)$	Sm (ppm)	Nd (ppm)	$^{147}Sm/^{144}Nd$	$^{143}Nd/^{144}Nd$ ±2σ	ε(t)Nd	$T(Nd)_{DM}$ (Ga)	$T(Nd)_{CHUR}$ (Ga)	$^{206}Pb/^{204}Pb$ ±2σ	$^{207}Pb/^{204}Pb$ ±2σ	$^{208}Pb/^{204}Pb$ ±2σ
98T69	30				0·70915 ± 2					0·512208 ± 5	−8·39			19·022 ± 3	15·732 ± 4	39·406 ± 8
98T70	30				0·70911 ± 2					0·512207 ± 8	−8·41			18·909 ± 3	15·655 ± 3	39·225 ± 6
98T71	30	127	6108	0·0821	0·70894 ± 3	0·708901	33·1	249·3	0·08060	0·512219 ± 7	−8·17	0·98	0·57	18·948 ± 2	15·676 ± 4	39·249 ± 1
98T73	30				0·70901 ± 2					0·512205 ± 6	−8·45			19·090 ± 2	15·800 ± 3	39·605 ± 5
Wenbu																
99T53	23	380	1442	0·7628	0·72216 ± 2	0·721909	27·5	206·6	0·08056	0·511883 ± 8	−14·96	1·34	1·01	18·480 ± 2	15·772 ± 6	39·520 ± 2
99T56	23	504	1155	1·2610	0·72218 ± 1	0·721768	33·9	253·5	0·08091	0·511888 ± 8	−14·87	1·34	1·00	18·881 ± 1	15·745 ± 8	39·288 ± 1
99T57	23	333	1847	1·2820	0·72438 ± 2	0·723958	36·4	253·5	0·07813	0·511875 ± 8	−15·11	1·32	1·07	18·421 ± 1	15·690 ± 2	39·300 ± 3
99T60	23	497	1122	0·5210	0·71845 ± 3	0·718279	27·1	210·0	0·08677	0·511893 ± 7	−14·79	1·31	0·98	18·420 ± 3	15·698 ± 4	39·271 ± 2
99T62	23	470	1513	0·8982	0·72052 ± 2	0·720227	28·7	208·9	0·08294	0·511893 ± 10	−14·78	1·35	1·02	18·453 ± 2	15·725 ± 4	39·438 ± 1
Chazi																
99T132	13	799	1593	1·4510	0·72036 ± 2	0·720089	31·8	159·9	0·12010	0·511985 ± 7	−12·94	1·70	1·32	18·808 ± 3	15·716 ± 6	39·431 ± 3
99T134	13	266	593	1·2960	0·71843 ± 2	0·718188	12·9	79·1	0·09859	0·512021 ± 10	−12·20	1·36	0·97	18·820 ± 4	15·733 ± 8	39·503 ± 3
99T145	13	600	794	2·1830	0·71820 ± 2	0·717797	17·4	98·2	0·10700	0·511996 ± 8	−12·70	1·49	1·11	18·948 ± 9	15·742 ± 1	39·633 ± 7
99T152	13	834	872	2·7650	0·71983 ± 1	0·719316	22·2	120·1	0·11160	0·511906 ± 7	−14·46	1·68	1·33	18·868 ± 4	15·750 ± 2	39·491 ± 1
99T154	13	317	1260	0·7267	0·71666 ± 1	0·716521	23·3	129·1	0·10920	0·511946 ± 6	−13·68	1·59	1·22	18·876 ± 6	15·765 ± 6	39·595 ± 5

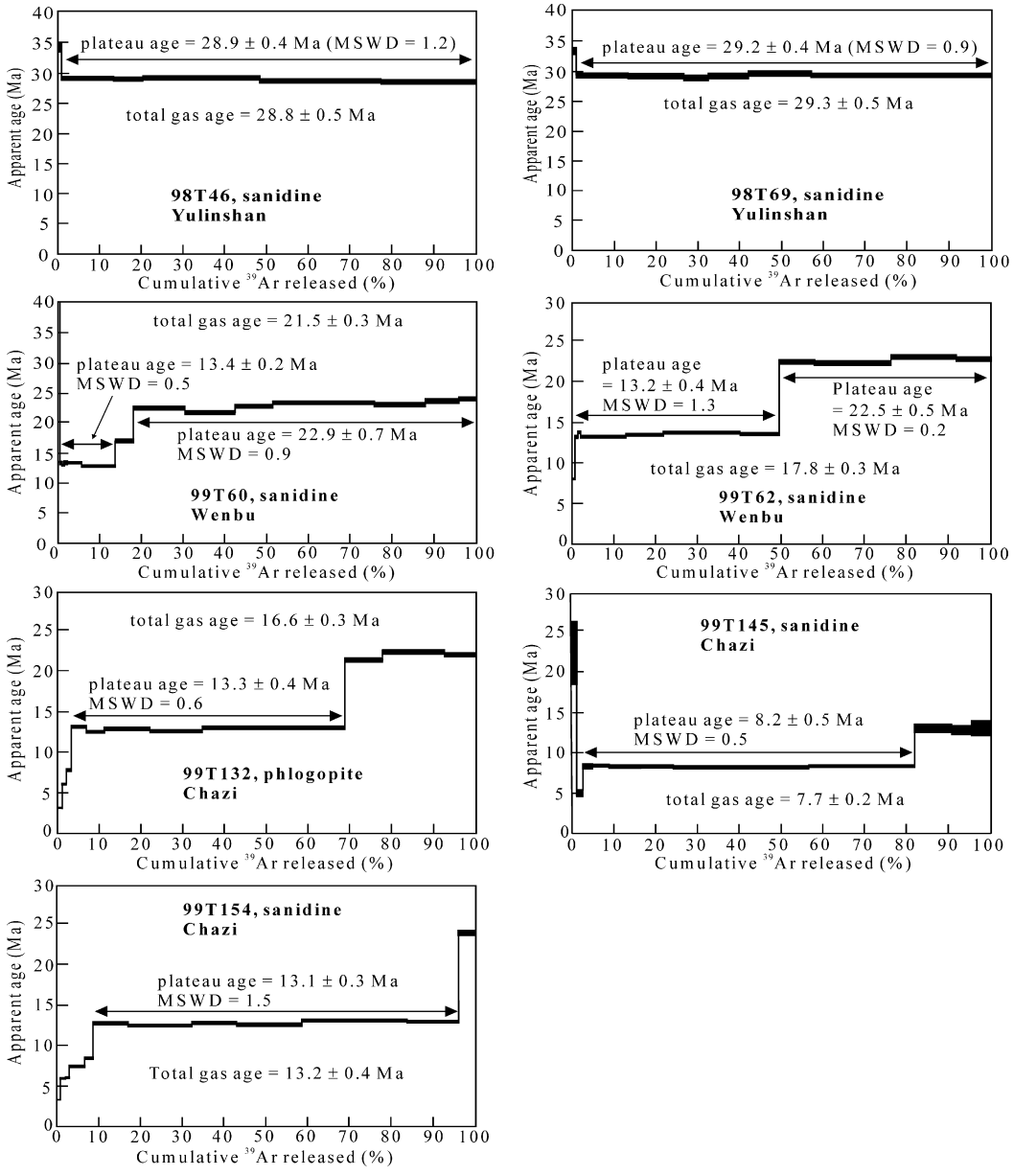

Fig. 5. $^{40}Ar/^{39}Ar$ step-heating release spectra.

8·2 ± 0·5 Ma (increments 3–8; 79% of ^{39}Ar released). These plateau ages are interpreted to represent the age of volcanism and are similar to the ages of volcanic rocks in the Majiang area, ~300 km along strike to the east (Fig. 1) (15–10 Ma; Coulon *et al.*, 1986).

PETROGRAPHY AND MINERALOGY

Lagala and Bangdaco

Studied samples of Lagala and Bangdaco volcanic rocks are weakly altered and dark green in colour. Phenocrysts (1–5% by volume) are composed entirely of olivine (1–2 mm in diameter), and the groundmass is composed of olivine + clinopyroxene + plagioclase + Fe–Ti oxides + glass (Table 3). Olivine phenocrysts in Lagala lavas have Fo contents of 84–70 wt %, whereas those in Bangdaco lavas have Fo contents of 85–80 wt %. Groundmass clinopyroxene has MgO contents of 15–13 wt %, with Al_2O_3 contents being higher for the Bangdaco lavas (9–8 wt %) than the Lagala lavas (6–4 wt %). Plagioclase in the groundmass is andesine or labradorite, with $An_{55–45}$ for Lagala lavas and $An_{52–50}$ for Bangdaco lavas.

Yulinshan

Yulinshan volcanic rocks can be divided into three main groups on the basis of phenocryst mineral assemblage: those that include (1) clinopyroxene + sanidine, but no leucite, (2) leucite + clinopyroxene + sanidine, and (3) either no phenocrysts or phenocrysts of mainly sanidine. As shown in the next section, these three groups correspond to trachyandesites (one of which is basaltic), tephriphonolites and trachytes, respectively.

Clinopyroxene- and sanidine-bearing samples that lack leucite may also include nosean, haüyne, nepheline and biotite phenocrysts. Their groundmass is composed of sanidine + clinopyroxene + nosean + apatite + glass. Some samples contain calcite amygdules that either exhibit chabazite reaction coronas with the groundmass or are completely replaced by chabazite. Clinopyroxene phenocrysts occur as aggregates and are chemically zoned. Rim compositions ($En_{18}Fs_{30}Wo_{52}$) are characterized by lower MgO and higher Na_2O than core compositions ($En_{23}Fs_{26}Wo_{51}$). Biotite phenocrysts are rich in TiO_2 (9 wt %) with *mg*-numbers [100Mg/(Mg + Fe)] of ~65. Sanidine is of the composition $Or_{65–75}Ab_{19–30}An_{1–5}$.

Leucite-bearing samples (leucite = 50–20 vol. %) include clinopyroxene (20–10 vol. %) and subordinate sanidine + haüyne + nosean + nepheline + sphene + biotite phenocrysts. The groundmass consists of clinopyroxene + sanidine + haüyne + nepheline + nosean + sphene + Fe–Ti oxide + glass. Leucite phenocrysts (2–10 mm in diameter) usually have two sets of polysynthetic twins with analcite reaction rims. Na_2O content in the leucite phenocrysts is <0·1 wt %. Nepheline phenocrysts (2–4 mm in diameter) are a solid solution of nepheline and kalsilite, with the chemical composition Na_2O 16–17 wt % and K_2O 4–5 wt %. Sanidine phenocrysts (2–5 mm in diameter) consist of $Or_{60–75}$ $Ab_{25–40}An_1$. Clinopyroxene phenocrysts (2–4 mm in diameter) exhibit distinct chemical zoning characterized by rims high in sodium. The chemical compositions of matrix minerals are similar to those of the phenocrysts.

Samples that contain no phenocrysts or phenocrysts of mainly sanidine exhibit typical trachytic textures. The groundmass is green-coloured and consists of microcrystalline sanidine + sodalite + aegirine + nepheline + magnesioriebeckite + glass. The composition of K-feldspar is similar to that of sanidine in the leucite-bearing assemblages. One sample contains phenocrysts of aegirine–augite, which are characterized by jadeite contents of up to 10 wt %.

Wenbu–Chazi

All five samples of the Wenbu volcanic neck contain phlogopite + clinopyroxene + sanidine ± leucite phenocrysts. The groundmass is composed of the same minerals as the phenocrysts, in addition to apatite + Fe–Ti oxide ± glass. Clinopyroxene phenocrysts ($Wo_{47}En_{47}Fs_6$ to $Wo_{45}En_{48}Fs_7$) are characterized by low Al_2O_3 (0·2–0·4 wt %). Phenocrystic and groundmass phlogopite are characterized by high *mg*-numbers (75–85).

Lavas in the Chazi area are characterized by phlogopite ± clinopyroxene ± sanidine phenocrysts and a glass-rich groundmass. Phenocrystic and groundmass phlogopite are characterized by high *mg*-numbers (80–85). Phenocrystic and groundmass clinopyroxene contain low TiO_2 (0·3–0·5) and Al_2O_3 (1·0–1·5) contents.

MAJOR AND TRACE ELEMENT GEOCHEMICAL DATA

Major elements

Major element data are summarized in Table 5. Lagala volcanic rocks have Na_2O (3·53–3·76 wt %) > K_2O (0·50–0·67 wt %), high MgO (8·80–9·48 wt %), and low SiO_2 (47·20–48·42 wt %) contents. They are slightly nepheline normative and classified as alkali basalts (Fig. 6a). Bangdaco lavas are characterized by low SiO_2 (~45 wt %) contents, moderate *mg*-numbers (54–55), and high Na_2O (4·6 wt %) and TiO_2 (2·1–2·2 wt %) contents. They are trachybasalts (Fig. 6a), and are further classified as sodic hawaiite because $Na_2O - 2 > K_2O$.

Yulinshan volcanic rocks are rich in K_2O (3–10 wt %) and relatively low in MgO (0·5–3·7 wt %). SiO_2 contents are variable (47·4–57·6 wt %) and decrease, whereas CaO (2·6–9·7 wt %) increases, with increasing MgO. Recalculated to 100% on an anhydrous basis, the rocks plot as basaltic trachyandesite, trachyandesite, tephriphonolite and trachyte on a $K_2O + Na_2O$ vs SiO_2 diagram (Fig. 6a), and within the leucitite and shoshonitic fields on a K_2O vs SiO_2 diagram (Fig. 6b). On a K_2O vs Na_2O diagram, the Yulinshan volcanic rocks plot in the ultrapotassic and shoshonitic fields (Fig. 6c). However, according to the definition of Foley *et al.* (1987), 98T52 is the only sample with high enough MgO (3·7 wt %) to be classified as ultrapotassic.

Wenbu volcanic rocks are characterized by high SiO_2 (57–60 wt %) and K_2O (8·6–11·7 wt %) contents, high *mg*-numbers (52–63) and high ratios of K_2O/Na_2O (3·8–9·2). All samples, except for 99T53 (MgO < 3 wt %), are ultrapotassic as defined by Foley *et al.* (1987). Chazi volcanic rocks are characterized by slightly lower K_2O (6·2–8·2 wt %) and a wider range in SiO_2 (50–69 wt %). MgO decreases from 7 wt % to 1·1 wt % with increasing SiO_2 content.

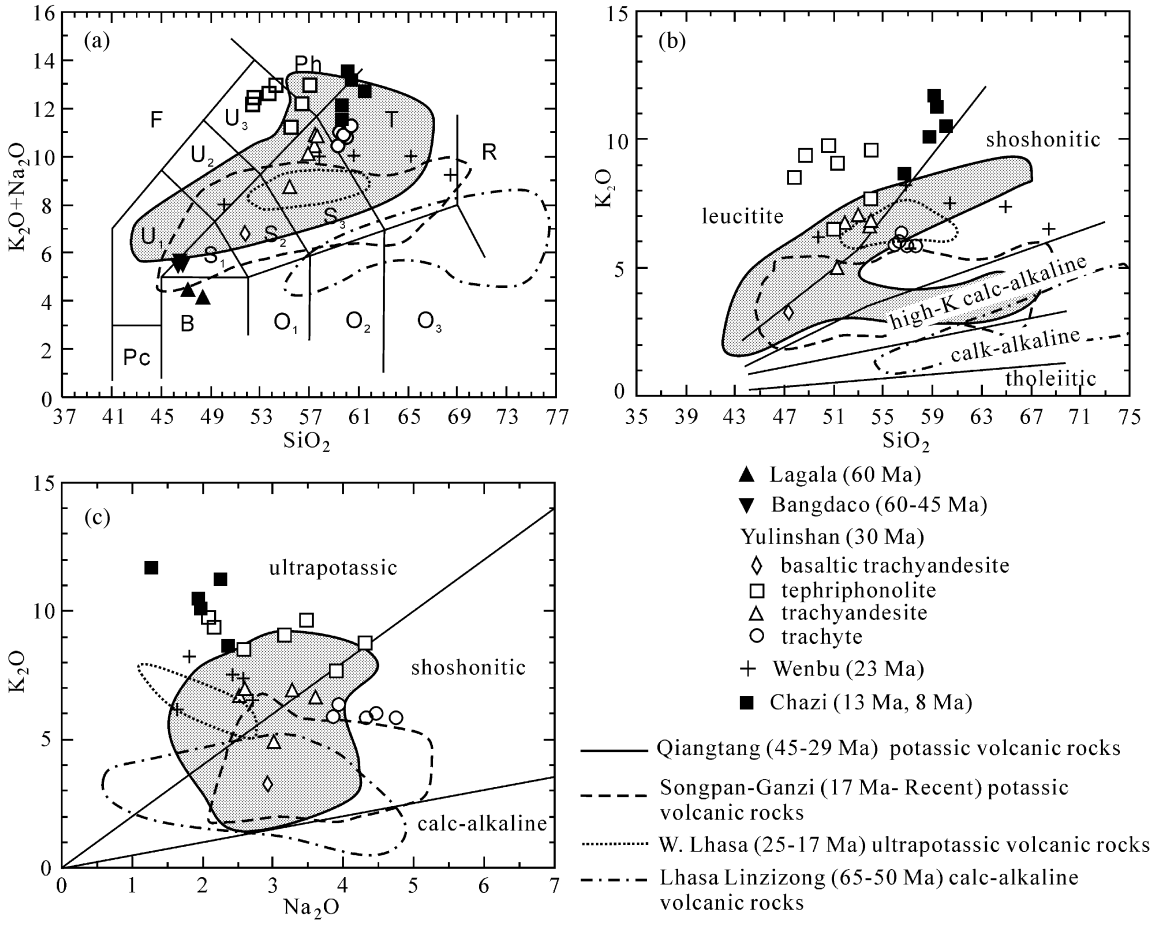

Fig. 6. (a) $K_2O + Na_2O$ vs SiO_2; classification from Le Bas *et al.* (1986); (b) K_2O vs SiO_2; (c) K_2O vs Na_2O plots for lavas analyzed in this study. Also plotted are potassic volcanic rocks from the Songpan–Ganzi, Qiangtang and western Lhasa terranes and Linzizong calc-alkaline volcanic rocks from the southern Lhasa terrane (Zheng *et al.*, 1986; Arnaud *et al.*, 1992; Turner *et al.*, 1993, 1996; Zhang, 1996; Deng, 1998; Miller *et al.*, 1999; Tan *et al.*, 2000; Lai & Liu, 2001; Dong, 2002). Pc, picrobasalt; B, basalt; O_1, basaltic andesite; O_2, andesite; O_3, dacite; R, rhyolite; S_1, trachybasalt; S_2, basaltic trachyandesite; S_3, trachyandesite; T, trachyte; U_1, basanite; U_2, phonotephrite; U_3, tephriphonolite; Ph, phonolite; F, foidite.

Recalculated to 100% on an anhydrous basis, the Chazi lavas plot in the fields of phonotephrite, trachyandesite and trachyte on a $K_2O + Na_2O$ vs SiO_2 diagram (Fig. 6a).

Trace elements

Trace element data are presented in Table 5. Lagala and Bangdaco volcanic rocks are slightly enriched in light rare earth elements (LREE; $La_n/Yb_n = 8–20$) and large ion lithophile elements (LILE). They exhibit chondrite-normalized REE variation patterns that are similar to those of Linzizong calc-alkaline volcanic rocks (Fig. 7a). A major difference, however, is the absence of a negative Eu anomaly for Lagala and Bangdaco volcanic rocks, which suggests either that plagioclase was not a major phase controlling magmatic differentiation or elevated f_{O_2}. Ta and Nb anomalies are weakly negative (Lagala) or absent (Bangdaco) and P and Ti anomalies are slightly positive (Fig. 7a). High concentrations of some of the compatible elements, such as Cr (Lagala, 768–839 ppm; Bangdaco, 204–215 ppm) and Ni (Lagala, 189–218 ppm; Bangdaco, 94–97 ppm) are suggestive of primitive magmatic characteristics.

Yulinshan volcanic rocks are characterized by very high REE and LILE (e.g. 96–604 ppm Rb; 5150–15880 ppm Sr; 1570–15970 ppm Ba; 33–219 ppm Th) contents—higher than most of the previously studied Cenozoic potassic volcanic rocks in Tibet (Fig. 7b). They have steep REE patterns ($La_n/Yb_n = 55–76$), although they are more enriched in heavy rare earth elements (HREE), such as Yb (>3 ppm), than other Tibetan potassic lavas. Compatible element contents are relatively low; Ni and Cr contents are in the range of 1–25 ppm and 16–61 ppm, respectively. The

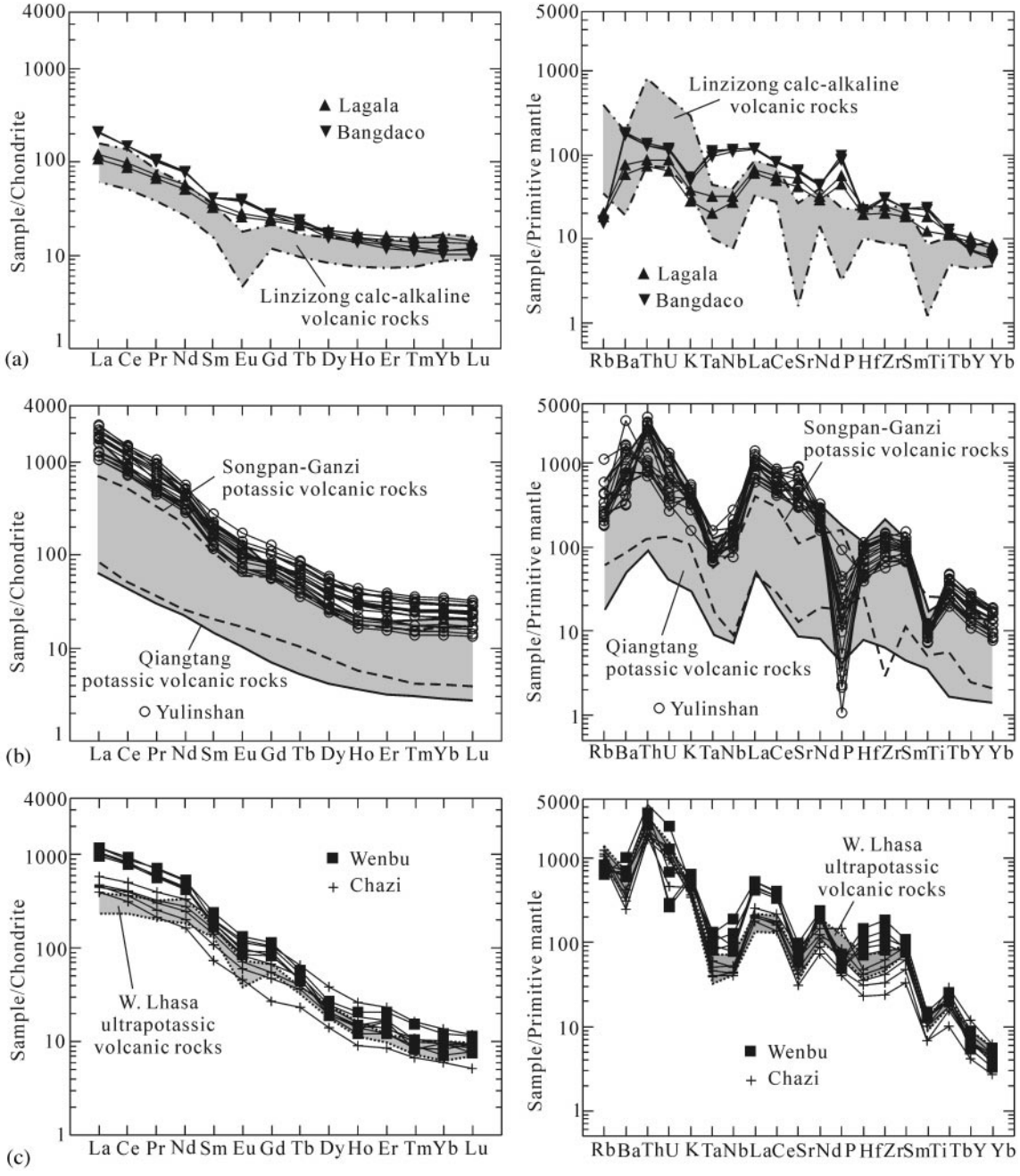

Fig. 7. Chondrite-normalized (Boynton, 1984) rare earth element diagrams and primitive mantle-normalized (Taylor & McLennan, 1985) trace element variation diagrams for volcanic rocks from the (a) Lagala and Bangdaco, (b) Yulinshan and (c) Wenbu–Chazi areas. Element order and normalizing values for the primitive mantle-normalized variation diagrams are from Sun & McDonough (1989). Shaded fields for volcanic rocks from other areas are based on the data sources listed in Fig. 6.

primary mantle-normalized variation diagrams are characterized by significant negative anomalies at Ta, Nb, P and Ti, despite their high concentrations (Fig. 7b).

Similar to the Yulinshan volcanic rocks, the Wenbu and Chazi lavas are highly enriched in LREE and LILE (e.g. 416–676 ppm Rb; 552–1760 ppm Sr; 1256–5160 ppm Ba; 108–283 ppm Th), with steep REE patterns (La_n/Yb_n = 41–139) (Fig. 7c). However, compatible element contents are higher than those of the Yulinshan lavas; Cr and Ni contents are in the range of 68–181 ppm and 44–117 ppm,

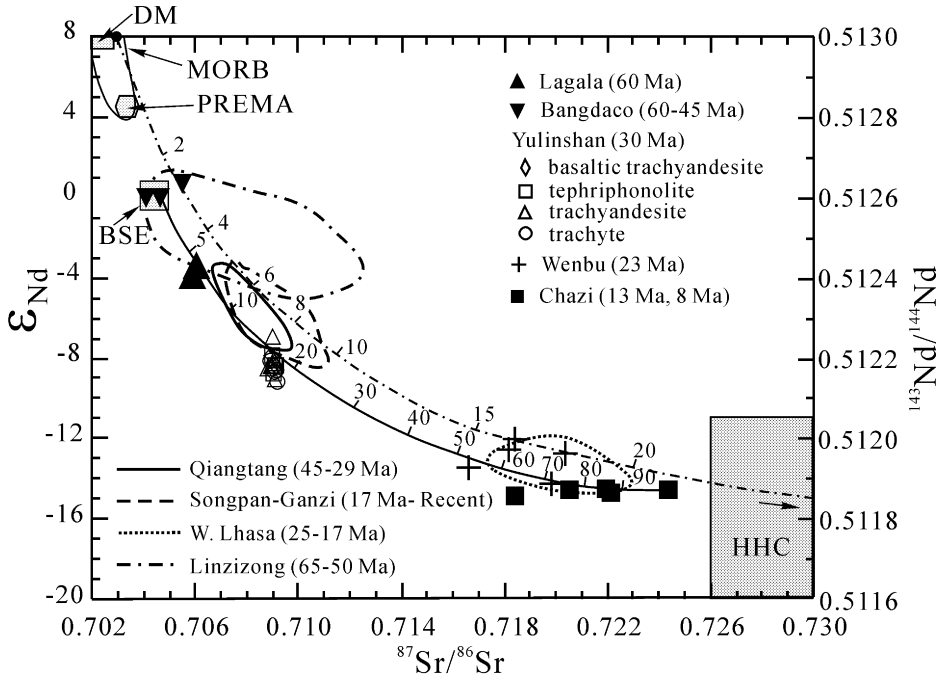

Fig. 8. $^{143}Nd/^{144}Nd$ vs $^{87}Sr/^{86}Sr$ for all the volcanic rocks analyzed in this study. Outlined fields for volcanic rocks from other areas are based on data sources listed in Fig. 6. The field for High Himalayan Crystalline rocks (HHC) is based on data from Harris (1995), Parrish & Hodges (1996), Robinson *et al.* (2001), Yang (2002) and Ding & Lai (2003); initial $^{87}Sr/^{86}Sr$ is up to 0·775 and plots outside the figure. The mantle sources of MORB and the mantle end-members DM, PREMA and BSE are from Zindler & Hart (1986). Fields for volcanic rocks from other areas are based on the data sources listed in Fig. 6. The dot–dash line is a mixing curve between depleted mantle (Taylor & McLennan, 1985; $^{87}Sr/^{86}Sr = 0{\cdot}703$, Sr = 20, $\varepsilon_{Nd} = +8$ and Nd = 1·2) and HHC (Ding & Lai, 2003; $^{87}Sr/^{86}Sr = 0{\cdot}775$, Sr = 31·28 and $\varepsilon_{Nd} = -18{\cdot}3$). The continuous line is a mixing curve between the Lhasa terrane ultrapotassic volcanic rocks (99T57) and the Bangdaco hawaiites (02T394) of this study.

respectively. Except for being characterized by higher LILE contents, the normalized REE and trace element variations for Wenbu and Chazi lavas, which include negative anomalies at Ta, Nb, P and Ti, are similar to those of ultrapotassic volcanic rocks in the western Lhasa terrane (Miller *et al.*, 1999).

Sr, Nd and Pb isotopes

Sr, Nd and Pb isotopic analyses are presented in Table 6. For Bangdaco, Wenbu, Chazi and two Yulinshan (99T15 and 99T71) samples, ratios of $^{87}Sr/^{86}Sr(i)$ and $^{143}Nd/^{144}Nd$ were age-corrected. Age-corrected Sr and Nd isotopic ratios differ by 0·01–0·07% and 0·001–0·002% from the uncorrected ratios, respectively. Sr and Nd isotopic ratios were not age-corrected for the Lagala and the remainder of the Yulinshan samples, for which $^{147}Sm/^{144}Nd$ and $^{87}Rb/^{86}Sr$ ratios were not measured. Likewise, Pb isotopic ratios for all samples were not age-corrected because $^{238}U/^{204}Pb$ and $^{232}Th/^{204}Pb$ ratios were not measured. These age-corrections would be expected to be minor, however, considering the young ages (~60 Ma and ~30 Ma) and low ratios of Rb/Sr (0·007–0·071), Sm/Nd (0·125–0·206) and U/Pb (0·04–0·18) for the samples.

Lagala volcanic rocks are characterized by $^{87}Sr/^{86}Sr$ and $^{143}Nd/^{144}Nd$ ratios of ~0·7060 and ~0·5124, respectively, and the following Pb isotopic ratios: $^{206}Pb/^{204}Pb$ 18·81–18·89, $^{207}Pb/^{204}Pb$ 15·56–15·60 and $^{208}Pb/^{204}Pb$ 38·89–38·96. The Bangdaco lavas exhibit less radiogenic $^{87}Sr/^{86}Sr$ (0·7040–0·7054), $^{207}Pb/^{204}Pb$ (15·50–15·53), $^{206}Pb/^{204}Pb$ (18·21–18·43) and $^{208}Pb/^{204}Pb$ (38·41–38·70), and higher $^{143}Nd/^{144}Nd$ ratios (~0·5126). The Sr, Nd and Pb isotopic ratios of Lagala and Bangdaco lavas are roughly similar to those of early Tertiary Linzizong volcanic rocks near Lhasa (Figs 8 and 9; Zhang, 1996; Dong, 2002). For Bangdaco lavas, Nd model ages relative to depleted mantle range from 0·57 to 0·64 Ga.

Yulinshan volcanic rocks are characterized by restricted and relatively high $^{87}Sr/^{86}Sr$ (0·7088–0·7092) and low $^{143}Nd/^{144}Nd$ (0·5121–0·5123) ratios that are similar to those of other potassic volcanic rocks in the Qiangtang terrane (Fig. 8). Nd model ages relative to depleted mantle were determined for two samples of Yulinshan lavas and are 1·03 Ga and 0·98 Ga. Pb isotopic ratios are

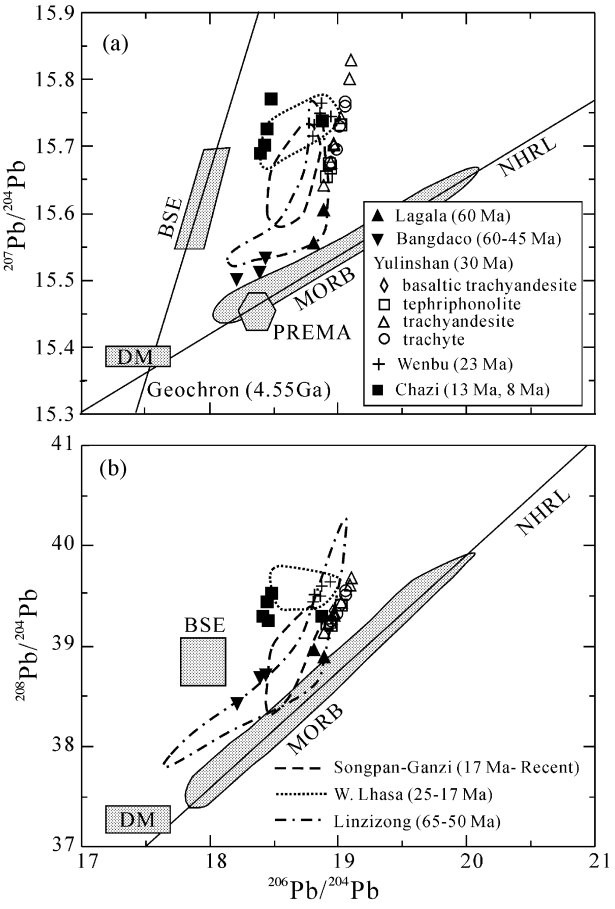

Fig. 9. (a) $^{207}Pb/^{204}Pb$ vs $^{206}Pb/^{204}Pb$ and (b) $^{208}Pb/^{204}Pb$ vs $^{206}Pb/^{204}Pb$ diagrams. Fields for volcanic rocks from other areas are based on the data sources listed in Fig. 6. The mantle sources of MORB and the mantle end-members DM, PREMA and BSE are from Zindler & Hart (1986).

radiogenic: $^{206}Pb/^{204}Pb = 18{\cdot}91–19{\cdot}10$, $^{207}Pb/^{204}Pb = 15{\cdot}64–15{\cdot}83$ and $^{208}Pb/^{204}Pb = 39{\cdot}14–39{\cdot}69$ (Fig. 9). On plots of $^{207}Pb/^{204}Pb$ and $^{208}Pb/^{204}Pb$ vs $^{206}Pb/^{204}Pb$ (Fig. 9), Yulinshan lavas yield steep arrays that lie significantly above the Northern Hemisphere Reference Line (NHRL), parallel to, but shifted to higher values of $^{206}Pb/^{204}Pb$ than the Geochron (4·55 Ga; Fig. 9a). The steep linear correlations between the different Pb isotopic ratios could be a result of within-run fractionation that was not adequately corrected for by factors determined through analysis of the international standard, NBS 981. However, similar linear correlations between Pb isotopic ratios have been determined for Tibetan potassic volcanic rocks by previous workers (e.g. Turner *et al.*, 1996; Miller *et al.*, 1999). Therefore, the uniform $^{206}Pb/^{204}Pb$ ratios and more variable $^{207}Pb/^{204}Pb$ and $^{208}Pb/^{204}Pb$ ratios are interpreted to be a characteristic of Tibetan potassic lavas as opposed to fractionation during analysis.

Wenbu and Chazi volcanic rocks are characterized by significantly higher $^{87}Sr/^{86}Sr$ (0·7165–0·7239) and lower $^{143}Nd/^{144}Nd$ (0·5118–0·5119) ratios than those of the Yulinshan volcanic rocks, but these values are similar to those of ultrapotassic volcanic rocks in the western Lhasa terrane (Fig. 8). Nd model ages relative to depleted mantle range between 1·31 and 1·35 Ga for Wenbu lavas and between 1·36 and 1·70 Ga for Chazi lavas. Ratios of $^{206}Pb/^{204}Pb$ (18·42–18·94), $^{207}Pb/^{204}Pb$ (15·69–15·77) and $^{208}Pb/^{204}Pb$ (39·27–39·63) for Wenbu and Chazi lavas are radiogenic and similar to those of the western Lhasa terrane rocks (Fig. 9).

DISCUSSION

Petrogenesis of Cenozoic volcanic rocks in central and southern Tibet

Lagala and Bangdaco

The Lagala and Bangdaco alkali basalts are relatively primitive, as demonstrated by their high contents of MgO (~9 wt % and ~7 wt %, respectively) and compatible elements such as Cr and Ni. Their parental magmas were clearly derived by partial melting of a mantle source. In contrast to the northern Qiangtang Bangdaco lavas, the southern Qiangtang Lagala lavas show slightly negative Nb and Ta anomalies (Fig. 7). This may indicate that the southern Qiangtang terrane mantle source included a subduction-related component. The latter could also account for the more radiogenic Sr and Nd isotopic ratios of the Lagala lavas relative to Bangdaco lavas. Alternatively, the Lagala lavas could have been derived from a mantle source that was isolated from the convecting asthenosphere for a longer period of time than that of the Bangdaco lavas.

On a Yb vs La/Yb diagram (Fig. 10) the Lagala, Bangdaco and Aksayqin (Deng, 1998) basalts lie roughly along a mixing trend (Langmuir *et al.*, 1978) between 4% partial melt of a hypothetical spinel-facies mantle and 0·1% partial melt of a hypothetical garnet-facies mantle. Quantitative modeling of REE abundance variations suggests that if the Lagala and Bangdaco magmas were derived from 3–4% melting of an assumed enriched mantle composition (La 1·19 ppm; Yb 0·31 ppm), the La contents of the partial melts would be 25–35 ppm (close to what is observed) for both the garnet-bearing and spinel-bearing mantle sources. However, the Yb contents would be ~0·5 ppm and 3–4 ppm for melts of a garnet-bearing and spinel-bearing mantle, respectively. Given these results, the Yb contents of Lagala (2·9–3·2 ppm) and Bangdaco (2·1–2·4 ppm) lavas may indicate that the parental magmas were derived largely from partial mantle melting within the spinel stability field. Minimal garnet in the mantle source is further supported by

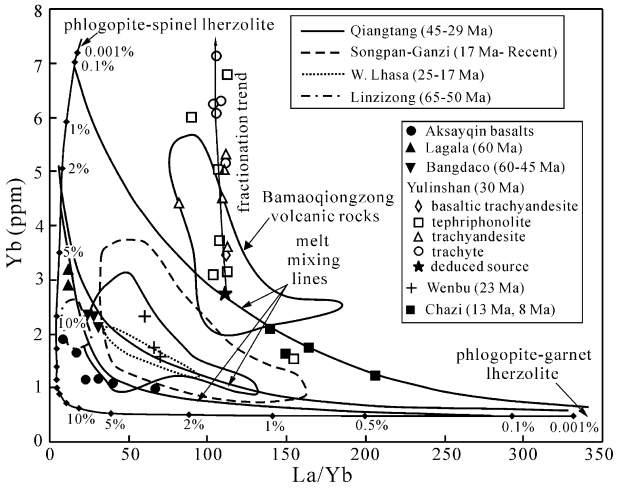

Fig. 10. Yb vs La/Yb diagram. Partial melting trends are indicated for phlogopite-bearing spinel and garnet lherzolite mantle sources, calculated using partition coefficients from Irving & Frey (1984) and McKenzie & O'Nions (1991). For phlogopite–spinel lherzolite, the assumed modal source mineralogy is Ol 0·55, Cpx 0·10, Opx 0·20, Sp 0·05 and Phl 0·10, and weight fractions of liquid contributed by each phase during melting are Ol 0·05, Cpx 0·20, Opx 0·10, Sp 0·20 and Phl 0·40. For phlogopite–garnet lherzolite, the assumed modal source mineralogy is Ol 0·55, Cpx 0·10, Opx 0·20, Gt 0·05 and Phl 0·10, and weight fractions of liquid contributed by each phase during melting are Ol 0·55, Cpx 0·25, Opx 0·20, Gt 0·40 and Phl 0·10. The assumed source composition is La 1·19 ppm and Yb 0·31 ppm, which is the composition of phlogopite–spinel lherzolite inclusions in high-pressure metamorphic rocks from the Eastern Himalayan syntaxis (Namche Barwa; Ding, 1999). Fields for volcanic rocks from other areas are based on the data sources listed in Fig. 6.

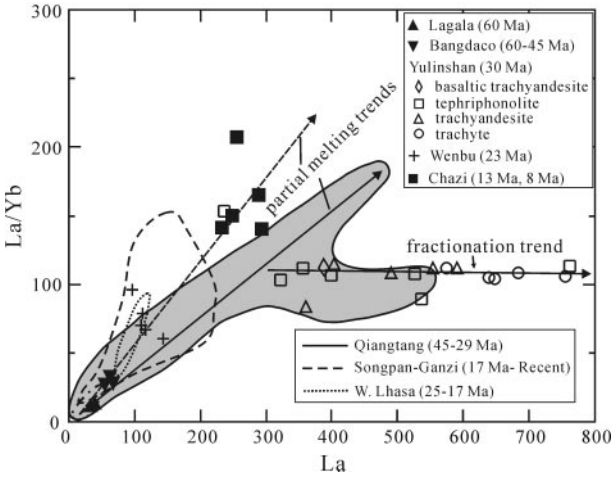

Fig. 11. Plot of La/Yb vs La for volcanic rocks analyzed in this study. Fields for volcanic rocks from other areas are based on the data sources listed in the caption of Fig. 6.

the similar chondrite-normalized concentrations of HREE (Er/Yb $\sim$ 1), as garnet fractionates Er from Yb and would be expected to yield Er/Yb $>$1.

Yulinshan

The low *mg*-numbers (4–47) and low Cr and Ni contents of the Yulinshan volcanic rocks (Table 4) indicate that they were derived from highly evolved magmas. On a plot of La/Yb vs La (Fig. 11), the small variation in La/Yb over a large range of La concentrations suggests that fractional crystallization played a major role in controlling chemical variation. Plots of La and Rb vs Ba (Fig. 12) allow evaluation of the relative importance of sanidine, leucite, nosean and clinopyroxene in the evolution of Yulinshan magmas. Significant decreases in Ba with moderate increases in La and minimal increases in Rb contents suggest that the compositions of the tephriphonolite, trachyandesite and highly evolved trachytic lavas were strongly influenced by fractional crystallization of sanidine. Analysis of tephriphonolite magmas suggests that their compositions may also have been influenced by fractional crystallization of clinopyroxene, leucite and perhaps nosean.

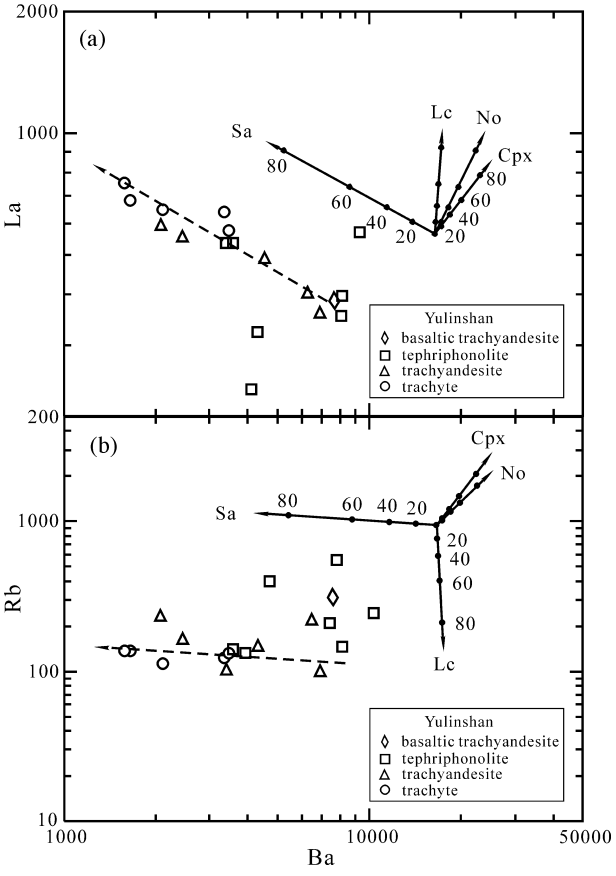

Fig. 12. (a) La vs Ba and (b) Rb vs Ba mineral vector diagrams showing inferred fractional crystallization trends (dashed arrows) for Yulinshan volcanic rocks. The partition coefficients for La, Rb and Ba in high-K rocks are from Francalanci *et al.* (1987) and the vectors were calculated from the Rayleigh fractionation equation. Cpx, clinopyroxene; Lc, leucite; No, nosean; Sa, sanidine.

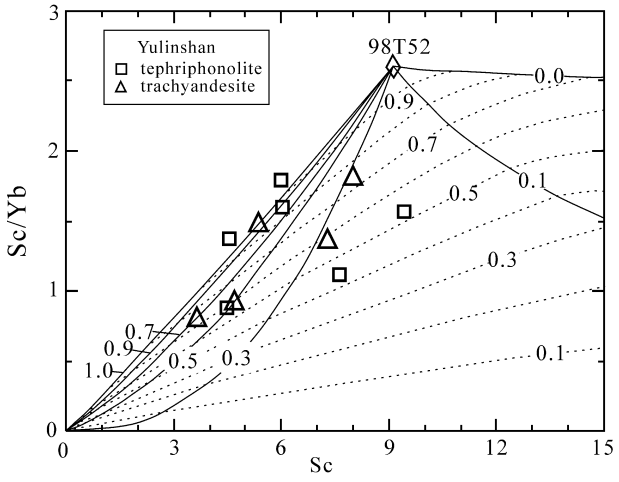

Fig. 13. Plot of Sc/Yb vs Sc, which shows fractional crystallization trends for Yulinshan lavas. The partition coefficients for Sc, Ba and Yb in high-K rocks are from Francalanci *et al.* (1987) and the fractional crystallization trends were calculated from the Rayleigh fractionation equation. The continuous lines are fractional crystallization trends for different ratios of the crystallizing phases (clinopyroxene: sanidine). The dashed lines show the fraction of melt remaining.

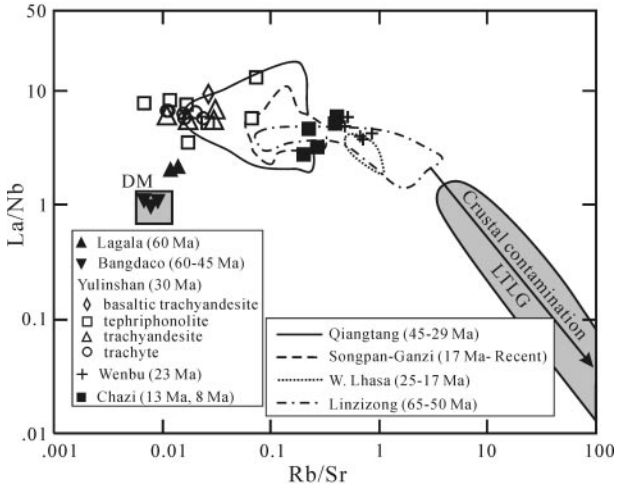

Fig. 14. Plot of La/Nb vs Rb/Sr. Depleted mantle (DM) is from Taylor & McLennan (1985) and the LTLG (Lhasa terrane leucogranite) field is based on compositions of Early Cretaceous (144–120 Ma) two-mica leucogranites in the northern Lhasa terrane (Harris *et al.*, 1988; Ding & Lai, 2003). Fields for volcanic rocks from other areas are based on the data sources listed in the caption of Fig. 6.

Ratios of a highly compatible element to an incompatible element as a function of the highly compatible element can be used to evaluate the extent of fractional crystallization in the petrogenesis of Yulinshan lavas (e.g. Sc/Yb vs Sc; Fig. 13). Sc and Ba are strongly compatible elements in clinopyroxene and incompatible in sanidine, whereas Yb is an incompatible element in clinopyroxene, sanidine and leucite. If the trachyandesite and tephriphonolite magmas are regarded to have undergone fractional crystallization from the most basic magma (assumed to be represented by sample 98T52), quantitative modelling of Sc/Yb vs Sc shows that trachyandesite and tephriphonolite lavas could be derived by 15–50% fractional crystallization of clinopyroxene and sanidine in ratios of Cpx/(Cpx + Sa) of 0·15–1·0 (Fig. 13).

Sr and Nd isotopic ratios are not affected by fractional crystallization. Therefore the uniform $^{87}Sr/^{86}Sr$ ($\sim$0·709) and $^{143}Nd/^{144}Nd$ ($\sim$0·5122) ratios for the Yulinshan lavas (Fig. 8) probably represent the isotopic characteristics of their source region. The extremely high contents of Sr and Nd would make the latter ratios insensitive to crustal contamination. The MgO content (3·6%) of the most mafic Yulinshan sample (basaltic trachyandesite) is sufficiently high to argue against the possibility that the potassic magmas were derived by partial melting of crustal rocks. For instance, the rhyolitic rocks of the Ulugh Muztagh area (Fig. 1), which are interpreted to be partial melts of pelitic lithologies, exhibit much lower MgO ($<$0·3%) as well as higher initial $^{87}Sr/^{86}Sr$ ratios ($\sim$0·715; McKenna & Walker, 1990). Furthermore, the extremely high concentrations of incompatible elements are not characteristic of typical upper crust or upper-crustal melts (Pearce *et al.*, 1984; Taylor & McLennan, 1985). On a La/Nb vs Rb/Sr diagram the Yulinshan lavas plot close to fields for mantle sources and do not show significant trends toward compositions of Cretaceous crustal-derived leucogranites in the northern Lhasa terrane (Fig. 14; Harris *et al.*, 1990; Ding & Lai, 2003). The extremely high concentrations of Sr and the absence of negative Eu anomalies suggest that plagioclase was not present in the source, and therefore probably reflect enrichment in the mantle source (e.g. Turner *et al.*, 1996).

The rather high K_2O, La and Ba contents of the least evolved Yulinshan lava (98T52; K_2O 3·2%, La 390 ppm and Ba 7600 ppm; Table 5) imply that high K_2O and LILE contents are also characteristic of their mantle source region (e.g. Turner *et al.*, 1996; Miller *et al.*, 1999). Possible potassic phases in the mantle source include phlogopite and K-rich amphibole, both of which can incorporate LILE in their structures (Konzett & Fei, 2000). As suggested for other Tibetan potassic lavas, the parent magmas of Yulinshan lavas were probably derived from small-degree partial melts of a strongly enriched mantle (Turner *et al.*, 1993, 1996; Deng, 1998; Miller *et al.*, 1999). The similar chondrite-normalized concentrations of HREE for the Yulinshan lavas suggest that garnet did not play a major role in their petrogenesis, as garnet fractionates Er from Yb to yield Er/Yb $>$1.

Wenbu–Chazi

The southern Tibetan Wenbu and Chazi ultrapotassic volcanic rocks are characterized by radiogenic Sr and unradiogenic Nd isotopic ratios, similar to those of ultrapotassic rocks in the western Lhasa terrane (Miller *et al.*, 1999). Their high *mg*-numbers (60–65) and high contents of compatible elements such as Cr (120–180 ppm) and Ni (70–120 ppm) indicate that they are more primitive than the Yulinshan lavas. As suggested for the western Lhasa terrane volcanic rocks (Miller *et al.*, 1999), it is unlikely that crustal assimilation and fractional crystallization processes (DePaolo, 1981) played a major role in the chemical evolution of the Wenbu and Chazi volcanic rocks. Assimilation of crustal material is inconsistent with the very high LILE and LREE contents and relatively low ratios of Rb/Sr for the Wenbu, Chazi and western Lhasa terrane ultrapotassic rocks (Fig. 10). Furthermore, the latter volcanic rocks yield a steeply sloping array on a La/Yb vs La diagram, which is characteristic of a partial melting trend and not a fractionation trend (Fig. 11). It is therefore concluded that the major and trace element compositions of the volcanic rocks were largely inherited from and reflect those within the mantle sources, with variations between samples being attributed to variable degrees of partial melting of the mantle source region. On a Yb vs La/Yb diagram (Fig. 14) the Wenbu volcanic rocks, along with the inferred parental magma of Yulinshan lavas, lie along a mixing trend between relatively small-degree partial melts of a spinel-facies phlogopite-bearing mantle (~0·1%) and a garnet-facies phlogopite-bearing mantle (~0·001%). The Chazi and western Lhasa terrane lavas may have been produced by higher degrees of partial melting, and lie roughly along a mixing trend between partial melts of a spinel-facies phlogopite-bearing mantle (~2%) and a garnet-facies phlogopite-bearing mantle (0·1%).

Nature and age of mantle metasomatism

The negative Nb, Ta and Ti anomalies in the incompatible element patterns of the Tibetan post-collisional potassic rocks (Fig. 7) suggest that subduction processes were probably responsible for metasomatism of their continental mantle source region (Arnaud *et al.*, 1992; Turner *et al.*, 1993, 1996; Deng, 1998; Miller *et al.*, 1999). The radiogenic Sr and Pb and unradiogenic Nd ratios of the potassic lavas depart drastically from those of the convecting asthenosphere, and the high La/Nb (2–10) and low ε_{Nd} (−5 to −15) values for most of the lavas cannot be produced by simple mixing of continental crust, oceanic island basalt (OIB) and asthenospheric magmas (Fig. 15). The geochemical and isotopic characteristics of Tibetan potassic lavas require strongly metasomatized mantle sources that were enriched in incompatible elements.

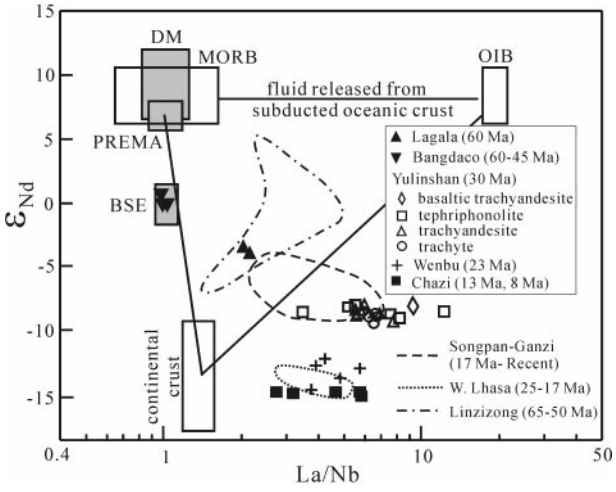

Fig. 15. ε_{Nd} vs La/Nb diagram. The MORB and mantle end-members BSE, DM and PREMA are from Zindler & Hart (1986). The composition of fluid released from subducted oceanic crust is estimated from the highest ε_{Nd} and La/Nb ratio measured for oceanic island basalts (OIB, White & Patchett, 1984). The continental crustal field is from Taylor & McLennan (1985). Fields for volcanic rocks from other areas are based on the data sources listed in Fig. 6.

It has been suggested that the Tibetan mantle lithosphere experienced a multi-stage history of metasomatism during Precambrian time, as inferred from Proterozoic Nd (0·9–1·3 Ga) and older Pb (2·2–3·5 Ga) model ages for Tibetan potassic volcanic rocks (e.g. Turner *et al.*, 1996; Miller *et al.*, 1999; this study). However, the possibility that an enriched Precambrian mantle lithosphere remained chemically isolated and physically intact beneath Tibet throughout Phanerozoic time is strongly questioned when the Phanerozoic tectonic and magmatic evolution of Tibet is considered.

The Tibetan terranes accreted to the southern margin of Asia primarily during Mesozoic time, following closure of major intervening ocean basins (e.g. Dewey *et al.*, 1988; Yin & Harrison, 2000). Northward subduction of Tethyan oceanic lithosphere along the Indus suture occurred over a time interval of at least 60 Myr before Indo-Asian collision (Xu *et al.*, 1985*a*; Miller *et al.*, 2000). It seems likely that subduction of multiple oceanic basins beneath Tibet during the Mesozoic would have significantly altered the chemical composition of any pre-existing Precambrian mantle lithosphere. Additionally, Triassic flysch of the Songpan–Ganzi terrane is interpreted to have been deposited largely on oceanic lithosphere (e.g. Sengör, 1987), and is suggested to have thrust southward directly beneath Qiangtang continental crust during early Mesozoic flat-slab oceanic subduction along the Jinsha suture (Kapp *et al.*, 2000, 2003*b*). Therefore if

the Qiangtang and Songpan–Ganzi terranes were underlain by enriched Precambrian mantle lithosphere during potassic volcanism, the above tectonic interpretations require the Precambrian lithosphere to be allochthonous and have underthrust this portion of Tibet subsequent to early Mesozoic time. Mid-Cretaceous northward flat-slab subduction of Tethyan oceanic lithosphere along the Indus suture has also been suggested (Coulon *et al*., 1986), and could have tectonically removed significant portions of the Lhasa terrane continental mantle lithosphere. An important consideration is the lack of pre-Eocene potassic volcanic rocks in Tibet; Cretaceous–Eocene volcanic rocks in the Lhasa terrane are calc-alkaline in composition (e.g. Coulon *et al*., 1986; Miller *et al*., 2000) whereas Paleocene–Eocene volcanic rocks in the Qiangtang terrane are alkaline (Deng, 1998; this study). There was ample opportunity for partial melting of Tibetan continental mantle lithosphere during Mesozoic tectonism. Oceanic slabs that were subducting during Mesozoic time probably experienced episodes of slab roll-back and break-off (e.g. Davies & von Blanckenburg, 1995), which would have provided heat sources for partial melting of the overlying mantle lithosphere. At least the Lhasa and Qiangtang terranes of Tibet experienced major crustal shortening (in excess of 50% for large regions) during Cretaceous time (Murphy *et al*., 1997; Kapp *et al*., 2002, 2003*a*). Early Cretaceous leucogranites in the northern Lhasa terrane represent high-temperature ($>850°C$) crustal melts and have been attributed to elevated heat input during attenuation of mantle lithosphere, which was previously overthickened during Mesozoic shortening (Harris *et al*., 1990).

It is here suggested that the Tibetan mantle lithosphere was metasomatized during Cenozoic time by subduction of ancient continental crust beneath Tibet during the Indo-Asian collision. The Precambrian Nd and Pb model ages inferred for Tibetan mantle lithosphere may not reflect the time when the lithosphere became isolated from asthenospheric convection, but rather isotopic signatures inherited from fluids and melts derived from subducted ancient continental crust. The concept of mantle metasomatism during Phanerozoic subduction of ancient continental material has previously been suggested to explain volcanic rocks with enriched and apparently ancient mantle sources in other collisional orogens (e.g. Hergt *et al*., 1989; Li, 1994; Jahn *et al*., 1999; Peccerillo, 1999).

On an ε_{Nd} vs $^{87}Sr/^{86}Sr$ diagram (Fig. 8), the Qiangtang alkali basalts and Tibetan potassic volcanic rocks lie roughly along mixing lines between (1) the two end-member lavas analyzed in this study: Bangdaco (02T394) and Wenbu (99T60), and (2) the depleted mantle and crust with high $^{87}Sr/^{86}Sr$ and low $^{143}Nd/^{144}Nd$ ratios, defined by the isotopic characteristics of the High Himalayan Crystallines (HHC; data from Harris, 1995; Parrish & Hodges, 1996; Robinson *et al*., 2001; Yang, 2002; Ding & Lai, 2003). This trend may suggest that the lithospheric mantle sources for the Tibetan potassic volcanic rocks were metasomatized by a continental crustal component (fluids and/or melts), similar in composition to the HHC. The isotopic compositions of Qiangtang (45–29 Ma) and Lhasa (25–8 Ma) terrane potassic magmas are consistent with their mantle sources having incorporated 5–10% and 15–20% of a continental crustal component, respectively (Fig. 8). Deviating from the mixing trend are the Linzizong calc-alkaline volcanic rocks, which provide an array toward more radiogenic Sr at lower Nd isotopic ratios (Zhang, 1996; Dong, 2002) (Fig. 8), characteristic of many island arc volcanic rocks (White & Patchett, 1984, and references therein). This observation is consistent with the hypothesis that the Lhasa terrane mantle lithosphere was not significantly metasomatized by continental material before the Indo-Asian collision. It is noted that the apparent mixing trend does not require mixing; it could be a consequence of the volcanic rocks having been derived from a Tibetan mantle lithosphere that is laterally heterogeneous in composition and history of metasomatism. However, the hypothesis of mantle metasomatism during Cenozoic continental subduction is consistent with: (1) the abrupt transition between alkaline and potassic volcanism in the Qiangtang terrane during Eocene time; (2) the trend toward more radiogenic Sr and less radiogenic Nd with decreasing age of the volcanic rocks in southern and central Tibet (more input of a continental component into the mantle source is expected to increase as Indo-Asian collision progresses); (3) the spatial and temporal distribution of Tertiary shortening and volcanism in Tibet (discussed in the next section). Additionally, it is unlikely that the apparent mixing trend is due to significant assimilation of crustal material into mantle-derived melts. This is because crustal assimilation would result in lower LILE and LREE contents than those measured for Tibetan potassic lavas and is inconsistent with the observation that LILE and LREE contents do not, in general, correlate negatively with *mg*-number (Turner *et al*., 1996; Miller *et al*., 1999).

Tectonic model for Cenozoic magmagenesis in Tibet (Fig. 16)

Before Indo-Asian collision, the Tethyan oceanic lithosphere may have been subducting northward beneath Tibet at a low angle (Coulon *et al*., 1986; Fig. 16a). Shortly before or during the initial stages of collision

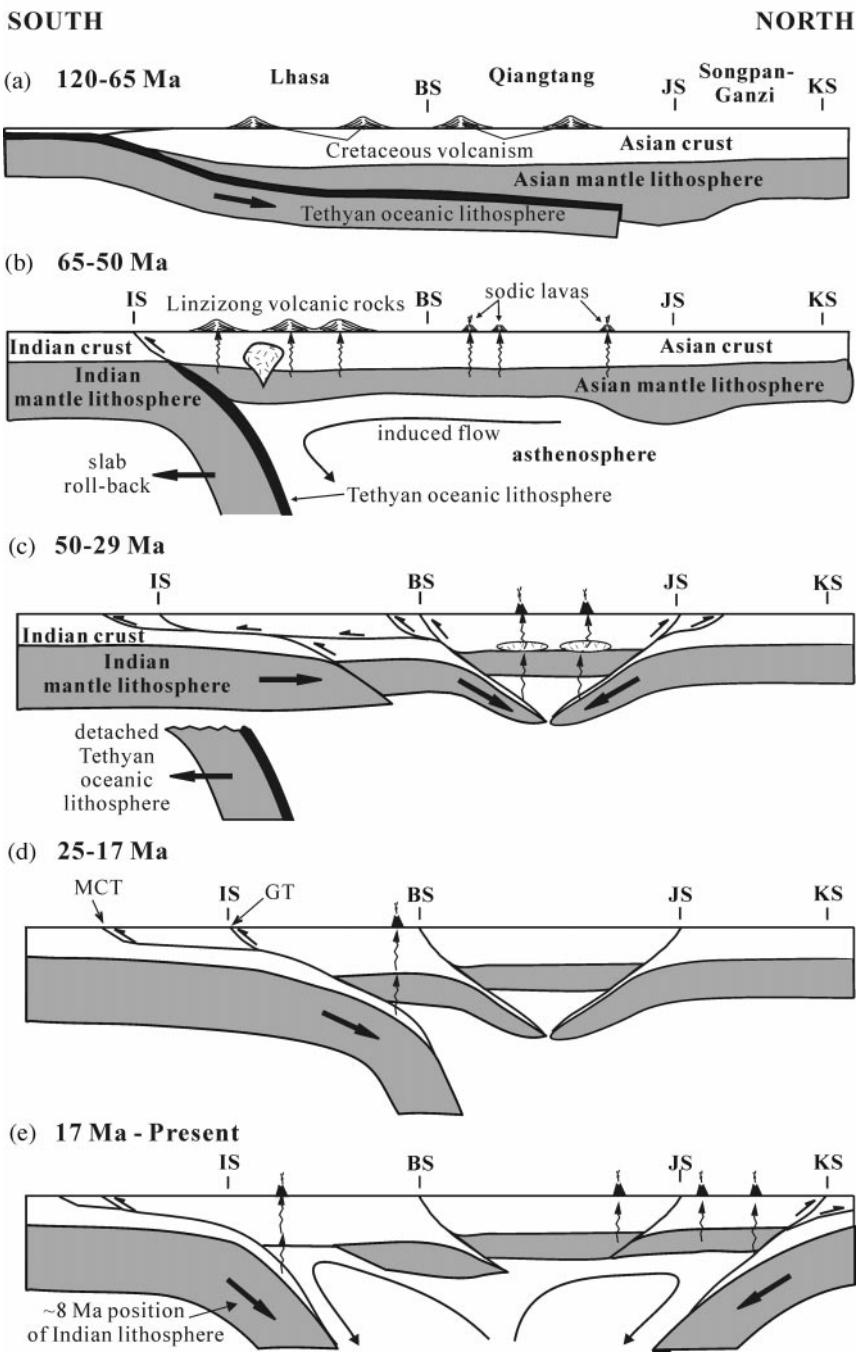

Fig. 16. Tectonic model for the genesis of Cenozoic volcanic rocks in Tibet. (a) 120–65 Ma: north-dipping, low-angle subduction of Tethyan oceanic lithosphere during a period of high plate convergence velocity (>100 mm/a; Dewey *et al.*, 1989). (b) 65–50 Ma: Early Tertiary alkaline volcanism in the Qiangtang terrane and Linzizong calc-alkaline volcanism in the Lhasa terrane occurred as a result of upwelling of asthenosphere that accompanied roll-back of the Tethyan oceanic slab. (c) 50–29 Ma: volcanism in the Qiangtang terrane is attributed to northward subduction of the Lhasa terrane and southward subduction of the Songpan–Ganzi terrane along the reactivated Bangong and Jinsha sutures, respectively (Tapponnier *et al.*, 2001). (d) 25–17 Ma: volcanism in the northern Lhasa terrane is attributed to northward subduction of Indian continental lithosphere along major thrust systems along and to the south of the Indus suture. (e) 17 Ma–present: volcanism in the southern Lhasa terrane is related to steepening of the northward-subducting Indian continental lithosphere. Volcanism in the Songpan–Ganzi terrane is coeval with southward subduction of Kunlun–Qaidam continental lithosphere along the Kunlun suture. Continental subduction may have forced convection in the asthenosphere, which in turn may have removed portions of the Songpan–Ganzi terrane mantle lithosphere and explain the broad distribution of volcanism. From (c) to (e), melts and fluids from the subducting ancient continental lithosphere metasomatized and induced partial melting of the overlying Tibetan continental mantle lithosphere, and resulted in the petrogenesis of Tibetan potassic lavas.

between India and Asia (poorly constrained to be between 70 and 50 Ma; see discussion by Yin & Harrison, 2000), the Tethyan oceanic slab may have undergone roll-back to steeper angles. Upwelling asthenosphere during slab roll-back may have initiated melting of Qiangtang upper mantle and produced the alkali basalts near the Lagala, Bangdaco and Aksayqin areas of the Qiangtang terrane, and the Linzizong volcanic rocks in the Lhasa terrane (Fig. 16b). This hypothesis of Cretaceous flat-slab oceanic subduction followed by earliest Tertiary roll-back is appealing because it would have provided a mechanism to remove significant portions of the Tibetan continental mantle lithosphere, which in turn would have facilitated India's northward underthrusting of southern Tibet during the Indo-Asian collision.

The convective thinning model of the lithosphere (Houseman *et al*., 1981; England & Houseman, 1986) has been widely used to explain the genesis of Tibetan post-collisional potassic volcanic rocks (McKenna & Walker, 1990; Molnar *et al*., 1993; Turner *et al*., 1993, 1996; Chung *et al*., 1998; Miller *et al*., 1999; Williams *et al*., 2001). According to this model, the ancient and enriched Tibetan continental mantle lithosphere was homogeneously thickened, along with the crust, during Cenozoic shortening. As a result of gravitational instability (mantle lithosphere is more dense than asthenosphere), portions of the continental mantle lithosphere were rapidly detached and replaced by upwelling of hot asthenosphere, which resulted in partial melting of the remaining sub-continental mantle lithosphere and regionally distributed potassic volcanism, as well as significant surface uplift. This model requires major crustal shortening to have pre-dated volcanism and a rather complicated temporal and spatial history of mantle removal to explain the age distribution of Tibetan potassic volcanic rocks (Fig. 1).

An alternative mechanism is fluid-fluxed melting of Tibetan mantle lithosphere during subduction of continental lithosphere along major Tertiary thrust systems (Deng, 1991; Arnaud *et al*., 1992; Meyer *et al*., 1998; Tapponnier *et al*., 2001; Wang *et al*., 2001). This mechanism predicts that there should be distinct belts of potassic magmatism that are parallel to and coeval with major thrust systems. Results of this study, when integrated with previous studies, strongly suggest that Middle Miocene and older Tibetan potassic volcanic rocks occur as roughly east–west-trending belts that are spatially associated with major thrust systems of similar age.

The documentation of ~30 Ma potassic volcanic rocks in the Yulinshan area of the western Qiangtang terrane helps better define an Eocene–Early Oligocene magmatic belt that is restricted to the Qiangtang terrane (Fig. 1). The Yulinshan volcanic rocks are folded and overlie conglomerate and sandstone that occur in the footwall of a thrust fault to the north (Fig. 2). Under the assumption that non-marine sedimentation was induced by thrust faulting, these structural observations suggest that upper-crustal shortening was occurring coeval with potassic volcanism. Major Paleocene to Oligocene thrusts systems and associated basinal strata (including volcanic interbeds) have also been documented along the Jinsha suture and in the northern Qiangtang terrane (Hoh Xil, Fenghuo Shan, and Nangqian–Yushu fold–thrust belts; Coward *et al*., 1988; Liu & Wang, 2001; Liu *et al*., 2001; Horton *et al*., 2002) and in the southern Qiangtang terrane and along the Bangong suture (Luo *et al*., 1996; Ai *et al*., 1998; Kapp *et al*., 2002, 2003*a*). The timing and spatial relationships between volcanism and thrusting favor a model in which Eocene–Oligocene potassic volcanism in the Qiangtang terrane is related to northward subduction of Lhasa terrane continental lithosphere and southward subduction of Songpan–Ganzi terrane continental lithosphere by reactivation of the Mesozoic Bangong and Jinsha sutures, respectively (Fig. 16c). Strong coupling between the Indian and Asian lithospheres could have been the driving mechanism for suture zone reactivation. Fluids and melts from subducted Songpan–Ganzi and Lhasa terrane crust could have metasomatized and catalyzed partial melting of mantle to produce the potassic lavas. Eocene–Oligocene potassic lavas in the central Qiangtang terrane differ from younger potassic lavas in that they are interpreted to have experienced major fractional crystallization (Yulinshan, Bamaoqiongzong, and Duoge–Cuoren areas; Lai & Liu, 2001; this study). This fractional crystallization probably occurred in crustal magma chambers, with rapid transport of magmas to the surface being impeded by coeval contraction within the upper crust.

The 25–17 Ma ultrapotassic rocks in the western Lhasa terrane and Wenbu area (~23 Ma) may be a part of a more extensive east–west-trending belt of magmatism within the northern Lhasa terrane. Major thrust systems of this age have not been documented in the northern Lhasa terrane, but are present along the Indus suture (Gangdese and Great Counter thrust system; e.g. Yin *et al*., 1994, 1999*a*; Harrison *et al*., 2000) and within the Himalaya (Tethyan thrust belt and Main Central Thrust; Ratschbacher *et al*., 1994; Hodges *et al*., 1996). Therefore, northward subduction of Indian continental lithosphere could have produced the 25–17 Ma ultrapotassic volcanism in the northern Lhasa terrane (Fig. 16d). The scarcity of upper-crustal contraction in the northern Lhasa terrane may have allowed mantle melts to transport rapidly through the crust without being affected

by significant crustal assimilation or fractional crystallization.

The ~8 Ma and ~13 Ma volcanic rocks in the Chazi area are potassic, in contrast to the ~16 Ma and 15–10 Ma calc-alkaline volcanic rocks that have been documented in SW Tibet (Miller *et al*., 1999) and near Majiang (Coulon *et al*., 1986), respectively. All of the volcanic rocks are associated with north-striking late Cenozoic rift systems (Pulan rift in SW Tibet, Murphy *et al*., 2002; Wenbu–Chazi rift, this study; Majiang rift, Kidd *et al*., 1988). Whereas rifting is suggested to have initiated in southern Tibet as early as ~18 Ma (Williams *et al*., 2001) or ~14 Ma (Coleman & Hodges, 1995), thermochronological studies near the Pulan (Murphy *et al*., 2002), Wenbu–Chazi (Stockli *et al*., 2002) and Majiang (Harrison *et al*., 1995) areas suggest that extension initiated later (10–8 Ma), subsequent to volcanism. Perhaps more significant than the structural setting of the volcanic rocks is the southward younging trend in volcanism, from 25–17 Ma in the northern Lhasa terrane to 16–8 Ma in the southern Lhasa terrane. This change in the age of magmatism may indicate steepening in the angle of the northward-subducting Indian lithosphere (Fig. 16e). The calc-alkaline volcanism may have occurred in areas of greater asthenospheric upwelling during slab roll-back.

Middle Miocene to Recent potassic volcanism is widely distributed in the Songpan–Ganzi terrane, and locally in the Bamaoqiongzong area of the northern Qiangtang terrane (Fig. 1). This volcanism was coeval with major crustal shortening within the Kunlun–Qaidam terrane to the north, which is proposed to have been accommodated in the continental mantle by southward subduction beneath the Songpan–Ganzi terrane (Deng, 1991; Meyer *et al*., 1998; Tapponnier *et al*., 2001). This inferred southward-dipping slab of Asian continental lithosphere has been recently well-imaged using seismic receiver functions (Kind *et al*., 2002), and probably played a major role in the metasomatism and partial melting of the northern Tibetan mantle lithosphere (Fig. 16e). The wide distribution of the northern Tibetan volcanism is striking, however, and may indicate that additional processes, such as convective thinning of the continental mantle lithosphere (e.g. Arnaud *et al*., 1992; Turner *et al*., 1996), may have acted to provide a more regional heat source.

CONCLUSIONS

The Lagala alkali basalts and Bangdaco hawaiites crystallized at 60–45 Ma and have high *mg*-numbers and high Cr and Ni contents characteristic of relatively primitive magmas. The Yulinshan volcanic rocks in the west–central Qiangtang terrane include basaltic trachyandesite, trachyandesite, tephriphonolite and trachyte, and crystallized at ~30 Ma. The Yulinshan lavas were derived from highly evolved magmas that experienced significant fractional crystallization. The Wenbu (~23 Ma) and Chazi (~13 Ma and ~8 Ma) ultrapotassic volcanic rocks in the central Lhasa terrane are less evolved than Yulinshan lavas, with high *mg*-numbers. The Yulinshan, Wenbu and Chazi volcanic rocks are characterized by radiogenic Sr and Pb, unradiogenic Nd isotopic ratios and strong enrichment in LILE and LREE. These characteristics probably reflect the enriched nature of their lithospheric mantle sources. Paleocene–Eocene alkaline volcanism in the Qiangtang terrane and calc-alkaline volcanism in the Lhasa terrane are attributed to earliest Tertiary roll-back of an initially shallow slab of northward subducting Tethyan oceanic lithosphere. A tectonic model in which the Tibetan mantle lithosphere was metasomatized and partially melted during Cenozoic subduction of ancient continental lithosphere is consistent with the timing and spatial distribution of post-collisional potassic volcanism and crustal shortening in Tibet.

ACKNOWLEDGEMENTS

We thank R. Xu, R. Zhang, H. Sang, J. Cao and P. Xu, Institute of Geology and Geophysics, Chinese Academy of Sciences, for assistance with major element, trace element, isotopic and electron microprobe analysis. D. M. Li at the Institute of Geology, China Seismological Bureau, assisted in K–Ar analysis. This work was supported by a grant from the Chinese National Key Project (1998040800) and Chinese Academy of Sciences grant (KZCXZ-SW-119). We thank A. Peccerillo, S. L. Chung and A. Yin for constructive comments on an early draft of this manuscript. We thank Tiffany Barry, Nick Rogers and an anonymous reviewer for their constructive reviews.

REFERENCES

Ai, H., Lan, L., Zhu, H., Zhang, K. & Zhen, T. (1998). The forming mechanism and petroleum geology of Tertiary Lunpola basin, southwest China. *Acta Petrolei Sinica* **19**, 21–27.

Allègre, C. J. & 34 others (1984). Structure and evolution of the Himalaya–Tibet orogenic belt. *Nature* **307**, 17–22.

Armijo, R., Tapponnier, P., Mercier, J. L. & Han, T. L. (1986). Quaternary extension in southern Tibet: field observations and tectonic implications. *Journal of Geophysical Research* **91**, 13803–13872.

Armijo, R., Tapponnier, P. & Han, T. (1989). Late Cenozoic right-lateral strike-slip faulting in southern Tibet. *Journal of Geophysical Research* **94**, 2787–2838.

Arnaud, N. O., Vidal, P., Tapponnier, P., Matte, Ph. & Deng, W. M. (1992). The high K_2O volcanism of northwestern

Tibet: geochemistry and tectonic implications. *Earth and Planetary Science Letters* **111**, 351–367.

Bird, P. & Toksoz, M. N. (1977). Strong attenuation of Rayleigh waves in Tibet. *Nature* **266**, 161–163.

Blisniuk, P. M., Hacker, B. R., Glodny, J., Ratschbacher, L., Bi, S., Wu, Z., McWilliams, M. O. & Calvert, A. (2001). Normal faulting in central Tibet since at least 13·5 Myr ago. *Nature* **412**, 628–632.

Boynton, W. V. (1984). Cosmochemistry of the rare earth elements: meteorite studies. In: Henderson, P. (ed.) *Rare Earth Element Geochemistry*. Amsterdam: Elsevier, pp. 63–114.

Brandon, C. & Romanowicz, B. (1986). A 'no-lid' zone in the Chang-Thang platform of Tibet: evidence from pure path phase velocity measurements of long period Rayleigh waves. *Journal of Geophysical Research* **91**, 6547–6564.

Bruguier, O., Lancelot, J. R. & Malavieille, J. (1997). U–Pb dating on single detrital zircon grains from the Triassic Sonpan–Ganze flysch (Central China): provenance and tectonic correlations. *Earth and Planetary Science Letters* **152**, 217–231.

Burchfiel, B. C., Molnar, P., Zhao, Z., Liang, K. U., Wang, S., Huang, M. & Sutter, J. (1989). Geology of the Ulugh Muztagh area, northern Tibet. *Earth and Planetary Science Letters* **94**, 57–70.

Burchfiel, B. C., Chan, Z., Liu, Y. & Royden, L. H., (1995). Tectonics of the Longmen Shan and adjacent regions, central China. *International Geology Review* **37**, 661–735.

Burg, J. P. & Chen, G. M. (1984). Tectonics and structural zonation of southern Tibet, China. *Nature* **311**, 219–223.

Burg, J.-P., Proust, F., Tapponnier, P. & Chen, G. M. (1983). Deformation phases and tectonic evolution of the Lhasa block (Southern Tibet, China). *Eclogae Geologicae Helvetiae* **76**, 643–665.

Catanzaro, E. J., Murphy, T. J., Shields, W. R. & Garner, E. L. (1968). Absolute isotopic abundance ratios of common equal-atom and radiogenic lead isotopic standards. *Journal of Research of the National Bureau of Standards A, Physics and Chemistry* **72A**, 261–267.

Chang, C. F. & Zheng, S. L. (1973). Tectonic features of the Mount Jolmo Lungma region in southern Tibet, China. *Scientia Geologica Sinica* **1**, 1–12 (in Chinese with English abstract).

Chen, W. P. & Molnar, P. (1981). Constraints on the seismic wave velocity structure beneath the Tibetan Plateau and their tectonic implications. *Journal of Geophysical Research* **86**, 5937–5962.

Cheng, J. & Xu, G. (1986). *Geologic map of the Gaize region at a scale of 1:1,000,000 and the geologic report*. Lhasa, Xizang Bureau of Geology and Mineral Resources, 369 pp. (in Chinese).

Chung, S. L., Lo, C. H., Lee, T. Y., Zhang, Y. Q., Xie, Y. W., Li, X. H., Wang, K. L. & Wang, P. L. (1998). Diachronous uplift of the Tibetan plateau starting 40 Myr ago. *Nature* **394**, 769–773.

Coleman, M. & Hodges, K. (1995). Evidence for Tibetan plateau uplift before 14 m.y. ago from a new minimum age for east–west extension. *Nature* **374**, 49–52.

Cooper, K. M., Reid, M. R., Dunbar, N. W. & McIntosh, W. C. (2002). Origin of mafic magmas beneath northwestern Tibet: constraints from 230Th–238U disequilibria. *Geochemistry, Geophysics, Geosystems* **3**, doi: 10.1029/2002GC000332.

Coulon, C., Maluski, H., Bollinger, C. & Wang, S. (1986). Mesozoic and Cenozoic volcanic rocks from central and southern Tibet: $^{39}Ar/^{40}Ar$ dating, petrological characteristics and geodynamical significance. *Earth and Planetary Science Letters* **79**, 281–302.

Coward, M. P., Kidd, W. S. F., Pan, Y., Shackleton, R. M. & Zhang, H. (1988). The structure of the 1985 Tibet Geotraverse, Lhasa to Golmud. *Philosophical Transactions of the Royal Society of London* **327**, 307–336.

Dalrymple, G. B. & Lanphere, M. A. (1969). *Potassium–Argon Dating*. San Francisco, CA: W. H. Freeman.

D'Andrea, J., Harrison, T. M., Grove, M. & Zhou, X. (1999). The thermal and physical state of the south Tibetan middle crust between 20–8 Ma: U–Th–Pb and Nd isotopic evidence from the Nyainqentanglha massif. In: Sobel, E., Appel, E., Strecker, M., Ratschbacher, L. & Blisniuk, P. (eds) *14th Himalaya–Karakoram–Tibet Workshop*. Kloster Ettal, Germany, p. 29.

Davies, J. H. & von Blanckenburg, F. (1995). Slab breakoff: a model of lithosphere detachment and deformation in collisional orogens. *Earth and Planetary Science Letters* **129**, 85–102.

Debon, F., Le Fort, P., Sheppard, S. M. & Sonet, J. (1986). The four plutonic belts of the Transhimalaya–Himalaya: a chemical, mineralogical, isotopic, and chronological synthesis along a Tibet–Nepal section. *Journal of Petrology* **27**, 219–250.

DeCelles, P. G., Robinson, D. M. & Zandt, G. (2002). Implications of shortening in the Himalayan fold–thrust belt for uplift of the Tibetan Plateau. *Tectonics* **21**, 1062, doi: 10.1029/2001tc001322.

Deng, W. M. (1989). Cenozoic volcanic rocks in the Northern Ngari district of Tibet—discussion on the concurrent intracontinental subduction. *Acta Petrologica Sinica* **3**, 1–11 (in Chinese with English abstract).

Deng, W. M. (1991). Cenozoic volcanism and intraplate subduction at the northern margin of the Tibetan Plateau. *Chinese Journal of Geochemistry* **10**, 140–152.

Deng, W. M. (1993). Study on trace element and Sr, Nd isotopic geochemistry of Cenozoic potassic volcanic rocks in north Tibet. *Acta Petrologica Sinica* **9**, 379–387 (in Chinese with English abstract).

Deng, W. M. (1998). *Cenozoic Intraplate Volcanic Rocks in the Northern Qinghai–Xizang Plateau*. Beijing: Geological Publishing House, pp. 1–180 (in Chinese with extended English abstract).

Deng, W. M., Sun, H. J. & Zhang, Y. Q. (2000). K–Ar age of the Cenozoic volcanic rocks in the Nangqen Basin, Qinghai Province and its geological significance. *Chinese Science Bulletin* **45**, 1015–1019.

DePaolo, D. (1981). Trace element and isotopic effects of combined wallrock assimilation and fractional crystallization. *Earth and Planetary Science Letters* **53**, 189–202.

Dewey, J. F. & Bird, J. M. (1970). Mountain belts and the new global tectonics. *Journal of Geophysical Research* **75**, 2625–2647.

Dewey, J. F., Shackleton, R. M., Chang, C. & Sun, Y. (1988). The tectonic evolution of the Tibetan Plateau. *Philosophical Transactions of the Royal Society of London, Series A* **327**, 379–413.

Dewey, J. F., Cande, S. & Pitman, W. C. (1989). Tectonic evolution of the India–Eurasia collision zone. *Eclogae Geologicae Helvetiae* **82**, 717–734.

Ding, L. (1999). Cenozoic collisional deformation and lithosphere tectonic evolution of the Eastern Himalayan syntaxis. Ph.D. dissertation, Institute of Geology and Geophysics, Chinese Academy of Sciences, Beijing, pp. 47–59.

Ding, L. & Lai, Q. (2003). New geological evidences of crust thickening in the Gangdese block prior to the Indo-Asian collision. *Chinese Science Bulletin* **48**, 836–842.

Dong, G. C. (2002). Linzizong volcanic rocks in Linzhou volcanic basin, Tibet: implications for India–Eurasia collision process. Ph.D. dissertation, China University of Geosciences, 134 pp.

England, P. & Houseman, G. (1986). Finite strain calculations of continental deformation 2. Comparison with the Indo-Asian collision zone. *Journal of Geophysical Research* **91**, 3664–3676.

Foley, S. F., Venturelli, G., Green, D. H. & Toscani, L. (1987). The ultrapotassic rocks: characteristics, classification, and constraints for petrogenetic models. *Earth-Science Reviews* **24**, 81–134.

Francalanci, F., Peccerillo, A. & Poli, G. (1987). Partition coefficients for minerals in potassium–alkaline rocks: data from Roman province (central Italy). *Geochemical Journal* **21**, 1–10.

Girardeau, J., Marcoux, J., Allègre, C. J., Bassoullet, J. P., Tang, Y., Xiao, X., Zao, Y. & Wang, X. (1984). Tectonic environment and geodynamic significance of the Neo-Cimmerian Donqiao ophiolite, Bangong–Nujiang suture zone, Tibet. *Nature* **307**, 27–31.

Hacker, B. R., Edwin, G., Ratschbacher, L., Grove, M., McWilliams, M., Sobolev, S., Jiang, W. & Wu, Z. H. (2000). Hot and dry deep crustal xenoliths from Tibet. *Science* **287**, 2463–2466.

Harris, N. (1995). Significance of weathering Himalayan metasedimentary rocks and leucogranites for the Sr isotope evolution of seawater during the early Miocene. *Geology* **23**, 795–798.

Harris, N. B. W., Xu, R., Lewis, C. L., Hawkesworth, C. J. & Zhang, Y. (1988). Isotope geochemistry of the 1985 Tibet Geotraverse, Lhasa to Golmud. *Philosophical Transactions of the Royal Society of London* **327**, 263–285.

Harris, N. B. W., Inger, S. & Xu, R. (1990). Cretaceous plutonism in Central Tibet: an example of post-collision magmatism? *Journal of Volcanology and Geothermal Research* **44**, 21–32.

Harrison, T. M., Copeland, P., Kidd, W. S. F. & Lovera, O. M. (1995). Activation of the Nyainqentanghla Shear Zone: implications for uplift of the southern Tibetan Plateau. *Tectonics* **14**, 658–676.

Harrison, T. M., Yin, A., Grove, M., Lovera, O. M., Ryerson, F. J. & Zhou, X. (2000). The Zedong Window: a record of superposed Tertiary convergence in southeastern Tibet. *Journal of Geophysical Research* **105**, 19211–19230.

Hergt, J. M., Chappell, B. W., McCulloch, M. T., McDougall, I. & Chivas, A. R. (1989). Geochemical and isotopic constraints on the origin of the Jurassic dolerites of Tasmania. *Journal of Petrology* **30**, 841–883.

Hirn, A., Jiang, M., Sapin, M., Diaz, J., Nercessian, A., Lu, Q. T., Lepine, J. C., Shi, D. N., Sachpazi, M., Pandey, M. R., Ma, K. & Gallart, J. (1995). Seismic anisotropy as an indicator of mantle flow beneath the Himalayas and Tibet. *Nature* **375**, 571–574.

Hodges, K. V., Parrish, R. R. & Searle, M. P. (1996). Tectonic evolution of the central Annapurna Range, Nepalese Himalayas. *Tectonics* **15**, 1264–1291.

Horton, B. K., Yin, A., Spurlin, M. S., Zhou, J. & Wang, J. (2002). Paleocene–Eocene syncontractional sedimentation in narrow lacustrine-dominated basins of east–central Tibet. *Geological Society of America Bulletin* **114**, 771–786.

Hou, L., Luo, D., Fu, D., Hu, S. & Li, K. (1991). *Triassic Sedimentary–Tectonic Evolution in Western Sichuan and Eastern Xizang Region*. Beijing: Geological Publishing House, 220 pp.

Houseman, G. A., McKenzie, D. P. & Molnar, P. (1981). Convective instability of a thickened boundary layer and its relevance for the thermal evolution of continental convergent belts. *Journal of Geophysical Research* **86**, 6115–6132.

Irving, A. J. & Frey, F. A. (1984). Trace element abundances in megacrysts and their host basalts: constraints on partition coefficients and megacryst genesis. *Geochimica et Cosmochimica Acta* **48**, 1201–1221.

Jahn, B. M., Wu, F. Y., Lo, C. H. & Tsai, C. H. (1999). Crust–mantle interaction induced by deep subduction of the continental crust: geochemical and Sr–Nd isotopic evidence from post-collisional mafic–ultramafic intrusions of the northern Dabie complex, central China. *Chemical Geology* **157**, 119–146.

Kapp, P., Yin, A., Manning, C. E., Murphy, M., Harrison, T. M., Spurlin, M., Ding, L., Deng, X. G. & Wu, C. M. (2000). Blueschist-bearing metamorphic core complexes in the Qiangtang block reveal deep crustal structure of northern Tibet. *Geology* **28**, 19–22.

Kapp, P., Yin, A., Harrison, T. M. & Ding, L. (2002). Cretaceous–Tertiary deformation history of central Tibet. *Geological Society of America, Abstracts with Programs* **34**, 487.

Kapp, P., Murphy, M. A., Yin, A., Harrison, T. M., Ding, L. & Guo, J. (2003*a*). Mesozoic and Cenozoic tectonic evolution of the Shiquanhe area of western Tibet. *Tectonics* (in press).

Kapp, P., Yin, A., Manning, C. E., Murphy, M. A., Harrison, T. M. & Ding, L. (2003*b*). Tectonic evolution of the early Mesozoic blueschist-bearing Qiangtang metamorphic belt, central Tibet. *Tectonics* (in press).

Kidd, W. S. F., Pan, Y., Chang, C., Coward, M. P., Dewey, J. F., F. R. S., Gansser, A., Molnar, P., Shackleton, R. M. & Sun, Y. (1988). Geological mapping of the 1985 Chinese–British Tibetan (Xizang–Qinghai) Plateau Geotraverse route. *Philosophical Transactions of the Royal Society of London* **327**, 287–305.

Kind, R., Yuan, X., Saul, J., Nelson, D., Sobolev, S. V., Mechie, J., Zhao, W., Kosarev, G., Ni, J., Achauer, U. & Jiang, M. (2002). Seismic images of crust and upper mantle beneath Tibet: evidence for Eurasian plate subduction. *Science* **298**, 1219–1221.

Kohn, M. J. & Parkison, C. D. (2002). Petrologic case for Eocene slab breakoff during the Indo-Asian collision. *Geology* **30**, 591–594.

Konzett, J. & Fei, Y. W. (2000). Transport and storage of potassium in the Earth's upper mantle and transition zone: an experimental study to 23 GPa in simplified and natural bulk compositions. *Journal of Petrology* **41**, 583–603.

Kosarev, G., Kind, R., Sobolev, S. V., Yuan, X., Hanka, W. & Oreshin, S. (1999). Seismic evidence for a detached Indian lithospheric mantle beneath Tibet. *Science* **283**, 1306–1309.

Lai, S. C. & Liu, C. Y. (2001). Enriched upper mantle and eclogitic lower crust in north Qiangtang, Qinghai–Tibet Plateau: petrological and geochemical evidence from the Cenozoic volcanic rocks. *Acta Petrologica Sinica* **17**, 459–468 (in Chinese with English abstract).

Langmuir, C. H., Vocke, R. D., Hanson, G. N. & Hart, S. R. (1978). A general mixing equation with applications to Icelandic basalt. *Earth and Planetary Sciences Letters* **37**, 380–392.

Le Bas, M. J., Le Maitre, R. W., Streckeisen, A. & Zanettin, B. (1986). A chemical classification of volcanic rocks based on the total alkali–silica diagram. *Journal of Petrology* **27**, 745–750.

Leeder, M. R., Smith, A. B. & Yin, J. (1988). Sedimentology and palaeoenvironmental evolution of the 1985 Lhasa to Golmud geotraverse. *Philosophical Transactions of the Royal Society of London* **327**, 107–143.

Lei, Q. L., Fu, X. Y. & Lu, Y. P. (1996). Petroleum geological features of Tertiary terrestrial Lunpola basin, Xizang (Tibet). *Earth Sciences—Journal of China University of Geosciences* **21**, 168–173 (in Chinese with English abstract).

Li, C. & Zheng, A. (1993). Paleozoic stratigraphy in the Qiangtang region of Tibet: relations of the Gondwana and Yangtze continents and ocean closure near the end of the Carboniferous. *International Geology Review* **35**, 797–804.

Li, C., Cheng, L. R., Hu, K., Yang, Z. R. & Hong, Y. R. (1995). *Study on the Paleo-Tethys Suture Zone of Lungmu Co-Shuanghu, Tibet*. Beijing: Geological Publishing House, pp. 1–131 (in Chinese with English abstract).

Li, S. G. (1994). Implications of ε_{Nd}–La/Nb, Ba/Nb, Nb/Th diagrams to mantle heterogeneity—classification of island arc basalts and decomposition of EMII component. *Geochimica* **32**, 106–114 (in Chinese with English abstract).

Liu, Z. & Wang, C. (2001). Facies analysis and depositional systems of Cenozoic sediments in the Hoh Xil basin, northern Tibet. *Sedimentary Geology* **140**, 251–270.

Liu, Z., Wang, C. & Yi, H. (2001). Evolution and mass accumulation of the Cenozoic Hoh Xil basin, northern Tibet. *Journal of Sedimentary Research* **71**, 971–984.

Liu, Z. Q. C. (1988). *Geologic Map of the Qinghai–Xizang Plateau and its Neighboring Regions (scale at 1:1,500,000)*. Beijing: Geological Publishing House.

Luo, B. J., Dai, G. Y. & Pan, Z. X. (1996). Oil and gas potential in Paleogene terrestrial Bangonghu–Dingqing suture zone. *Earth Sciences—Journal of China University of Geosciences* **21**, 164–167 (in Chinese with English abstract).

Maheo, G., Guillot, S., Blichert-Toft, J., Rolland, Y. & Pecher, A., (2002). A slab breakoff model for the Neogene thermal evolution of South Karakorum and South Tibet. *Earth and Planetary Science Letters* **195**, 45–58.

Maluski, H., Proust, F. & Xiao, X. C. (1982). $^{39}Ar/^{40}Ar$ dating of the trans-Himalayan calc-alkaline magmatism of southern Tibet. *Nature* **298**, 152–154.

McKenna, L. W. & Walker, J. D. (1990). Geochemistry of crustally derived leucocratic igneous rocks from the Ulugh Muztagh area, Northern Tibet and their implications for the formation of the Tibetan Plateau. *Journal of Geophysical Research* **95**, 21483–21502.

McKenzie, D. & O'Nions, R. K. (1991). Partial melt distributions from inversion of rare earth element concentrations. *Journal of Petrology* **32**, 1021–1091.

Meyer, B., Tapponnier, P., Bourjot, L., Métevier, F., Gaudemer, Y., Peltzer, G., Guo, S. & Chen, Z. (1998). Crustal thickening in Gansu–Qinghai, lithospheric mantle subduction, and oblique, strike-slip controlled growth of the Tibet plateau. *Geophysical Journal International* **135**, 1–47.

Michard, A., Gurriet, P., Soudant, M. & Albarède, F. (1985). Nd isotopes in French Phanerozoic shales: external vs. internal aspects of crustal evolution. *Geochimica et Cosmochimica Acta* **49**, 601–610.

Miller, C., Schuster, R., Klotzli, U., Frank, W. & Purtscheller, F. (1999). Post-collisional potassic and ultrapotassic magmatism in SW Tibet: geochemical and Sr–Nd–Pb–O isotopic constraints for mantle source characteristics and petrogenesis. *Journal of Petrology* **40**, 1399–1424.

Miller, C., Schuster, R., Klötzli, U., Frank, W. & Grasemann, B. (2000). Late Cretaceous–Tertiary magmatic and tectonic events in the Transhimalaya batholith (Kailas area, SW Tibet). *Schweizerische Mineralogische und Petrographische Mitteilungen* **80**, 1–20.

Molnar, P., England, P. & Martinod, J. (1993). Mantle dynamics, uplift of the Tibetan Plateau, and the Indian monsoon. *Reviews of Geophysics* **31**, 357–396.

Murphy, M. A., Yin, A., Harrison, T. M., Dürr, S. B., Chen, Z., Ryerson, F. J., Kidd, W. S. F., Wang, X. & Zhou, X. (1997). Did the Indo-Asian collision alone create the Tibetan plateau? *Geology* **25**, 719–722.

Murphy, M. A., Yin, A., Kapp, P., Harrison, T. M., Manning, C. E., Ryerson, F. J., Ding, L. & Guo, J. (2002). Structural and thermal evolution of the Gurla Mandhata detachment system, southwest Tibet: implications for the eastward extent of the Karakoram fault system. *Geological Society of America Bulletin* **114**, 428–447.

Nelson, K. D., Zhao, W. J., Brown, L. D., Kuo, J., Che, J. K., Liu, X. W., *et al*. (1996). Partially molten middle crust beneath Southern Tibet: synthesis of Project INDEPTH results. *Science* **274**, 1684–1696.

Nie, S., Yin, A., Rowley, D. B. & Jin, Y. (1994). Exhumation of the Dabie Shan ultra-high pressure rocks and accumulation of the Songpan–Ganzi flysch sequence, central China. *Geology* **22**, 999–1002.

Owens, T. J. & Zandt, G. (1997). Implications of crustal property variations for models of Tibetan plateau evolution. *Nature* **387**, 37–43.

Pan, Y. (1993). Unroofing history and structural evolution of the southern Lhasa terrane, Tibetan Plateau: implications for the continental collision between India and Asia. Ph.D. thesis, State University of New York, Albany.

Parrish, R. R. & Hodges, K. V. (1996). Isotopic constraints on the age and provenance of Lesser and Greater Himalayan sequences, Nepalese Himalaya. *Geological Society of America Bulletin* **108**, 904–911.

Pearce, J. A. & Deng, W. (1988). The ophiolites of the Tibetan Geotraverses, Lhasa to Golmud (1985) and Lhasa to Kathmandu (1986). *Philosophical Transactions of the Royal Society of London* **327**, 215–238.

Pearce, J. A. & Mei, H. J. (1988). Volcanic rocks of the 1985 Tibet geotraverse, Lhasa to Golmud. The geological evolution of Tibet. *Philosophical Transactions of the Royal Society of London* **327**, 169–201.

Pearce, J. A., Harrison, N. B. & Tindle, A. G. (1984). Trace element discrimination diagrams for tectonic interpretation of granitic rocks. *Journal of Petrology* **25**, 956–983.

Peccerillo, A. (1999). Multiple mantle metasomatism in central–southern Italy: geochemical effects, timing and geodynamic implications. *Geology* **27**, 315–318.

Quidelleur, X., Grove, M., Lovera, O. M., Harrison, T. M. & Yin, A. (1997). Thermal evolution and slip history of the Renbu–Zedong Thrust, southeastern Tibet. *Journal of Geophysical Research* **102**, 2659–2679.

Rao, R., Xu, J., Chen, Y. & Zou, D. (1987). *The Triassic System of the Qinaghai–Xizang Plateau*. Beijing: Geological Publishing House, 239 pp.

Ratschbacher, L., Frisch, W., Liu, G. & Chen, C. C. (1994). Distributed deformation in southern and western Tibet during and after the India–Asian collision. *Journal of Geophysical Research* **99**, 19917–19945.

Renne, P. R., Deino, A. L., Walter, R. C., Turrin, B. D., Swisher, C. C., Becker, T. A., Curtis, G. H., Sharp, W. D. & Jaouni, A. R. (1994). Intercalibration of astronomical and radioisotopic time. *Geology* **22**, 783–786.

Robinson, D. M., DeCelles, P. G., Patchett, P. J. & Garzione, C. N. (2001). The kinematic evolution of the Nepalese Himalaya interpreted from Nd isotopes. *Earth and Planetary Science Letters* **192**, 507–521.

Roger, F., Tapponnier, P., Arnaud, N., Schärer, U., Brunel, M., Xu, Z. & Yang, J. (2000). An Eocene magmatic belt across central Tibet: mantle subduction triggered by the Indian collision? *Terra Nova* **12**, 102–108.

Sengör, A. M. C. (1984). *The Cimmeride Orogenic System and the Tectonics of Eurasia*. *Geological Society of America, Special Papers* **195**, 88 pp.

Sengör, A. M. C. (1987). Tectonic subdivisions and evolution of Asia. *Bulletin of the Technical University of Istanbul* **40**, 355–435.

Steiger, R. H. & Jäger, E. (1977). Subcommission on geochronology: convention on the use of decay constants in geo- and cosmochronology. *Earth and Planetary Science Letters* **36**, 359–362.

Stockli, D., Taylor, M., Yin, A., Harrison, T. M., D'Andrea, J., Kapp, P. & Ding, L. (2002). Late Miocene–Pliocene inception of E–W extension in Tibet as evidenced by apatite (U–Th)/He data. *Geological Society of America, Abstracts with Programs* **34**, 411.

Sun, S. S. & McDonough, W. F. (1989). Chemical and isotopic systematics of oceanic basalts: implications for mantle composition and processes. In: Saunders, A. D. & Norry, M. J. (eds) *Magmatism in the Ocean Basins*. *Geological Society, London, Special Publications* **42**, 313–345.

Tan, F. W., Pan, G. T. & Xu, Q. (2000). The uplift of Qinghai–Xizang Plateau and geochemical characteristics of Cenozoic volcanic rocks from the center of Qiangtang, Xizang. *Acta Petrologica et Mineralogica* **19**, 121–130 (in Chinese with English abstract).

Tang, Y. & Wang, F. (1984). Primary analysis of the tectonic environment of the ophiolite in Northern Xizang. *Himalayan Geology* **2**, 99–113 (in Chinese).

Tapponnier, P. & Molnar, P. (1977). Active faulting and tectonics in China. *Journal of Geophysical Research* **82**, 2905–2930.

Tapponnier, P. & 29 others (1981). The Tibetan side of the India–Eurasia collision. *Nature* **294**, 405–410.

Tapponnier, P., Xu, Z. Q., Roger, F., Meyer, B., Arnaud, N., Wittlinger, G. & Yang, J. S. (2001). Oblique stepwise rise and growth of the Tibet Plateau. *Science* **294**, 1671–1677.

Taylor, M., Yin, A., Ryerson, F. J., Kapp, P. & Ding, L. (2003). Conjugate strike-slip faulting along the Bangong–Nujiang suture zone accommodates coeval east–west extension and north–south shortening in the interior of the Tibetan Plateau. *Tectonics* (in press).

Taylor, S. R. & McLennan, S. M. (1985). *The Continental Crust: its Composition and Evolution*. Oxford: Blackwell Scientific.

Turner, S., Hawkesworth, C. J., Liu, J., Rogers, N., Kelley, S. & van Calsteren, P. (1993). Timing of Tibetan uplift constrained by analysis of volcanic rocks. *Nature* **364**, 50–53.

Turner, S., Arnaud, N., Liu, L., Rogers, N., Hawkesworth, C., Harris, N., Kelley, S., Van Calsteren, P. & Deng, W. M. (1996). Post-collision, shoshonitic volcanism on the Tibetan Plateau: implications for convective thinning of the lithosphere and the source of ocean island basalts. *Journal of Petrology* **37**, 45–71.

Wang, C., Liu, Z., Yi, H., Liu, S. & Zhao, X. (2002). Tertiary crustal shortening and peneplanation in the Hoh Xil region: implications for the tectonic history of the northern Tibetan Plateau. *Journal of Asian Earth Sciences* **20**, 211–223.

Wang, J.-H., Yin, A., Harrison, T. M., Grove, M., Zhang, Y.-Q. & Xie, G.-H. (2001). A tectonic model for Cenozoic igneous activities in the eastern Indo-Asian collision zone. *Earth and Planetary Science Letters* **188**, 123–133.

Wang, S. (1980).The features of the Linzizong volcanic series in the eastern section of the Gangdise volcanic arc in Xizang (Tibet). In: *Mission Franco-Chinois au Tibet*. Beijing: Geological Publishing House, pp. 305–320 (in Chinese with English abstract).

Wang, S. (1992). Constraints of chlorine on $^{40}Ar/^{39}Ar$ dating and calculation of high-precise $^{40}Ar/^{39}Ar$ ages. *Scientia Geologica Sinica* **27**, 369–378 (in Chinese with English abstract).

Wang, S., Li, Z. & Xiyao, Q. (1983). *Geologic map of the Xigaze region at a scale of 1:1000,000 and the geologic report*. Lhasa: Xizang Bureau of Geology and Mineral Resources, pp. 301–309 (in Chinese).

Wang, S., Sang, H. & Hu, S. (1985). $^{40}Ar/^{39}Ar$ age determinant using 49-2 reactor and $^{40}Ar/^{39}Ar$ age spectrum for amphibolite from Qianan, China. *Acta Petrologica Sinica* **2**, 35–44 (in Chinese with English abstract).

Wei, W., Unsworth, M., Jones, A., Booker, J., Tan, H., Nelson, D., Chen, L., Li, S., Solon, K., Bedrosian, P., Jin, S., Deng, M., Ledo, J., Kay, D. & Roberts, B. (2001). Detection of widespread fluids in the Tibetan crust by magnetotelluric studies. *Science* **292**, 716–718.

White, W. M. & Patchett, J. (1984). Hf–Nd–Sr isotopes and incompatible element abundances in island arcs: implications for magma origins and crust–mantle evolution. *Earth and Planetary Science Letters* **67**, 167–185.

Williams, H., Turner, S., Kelley, S. & Harris, N. (2001). Age and composition of dikes in Southern Tibet: new constraints on the timing of east–west extension and its relationship to postcollisional volcanism. *Geology* **29**, 339–342.

Xu, R.-H., Schärer, U. & Allègre, C. J. (1985*a*). Magmatism and metamorphism in the Lhasa block (Tibet): a geochronological study. *Journal of Geology* **93**, 41–57.

Xu, Z. Y., Zhao, J. P. & Wu, Z. L. (1985*b*). On the Tertiary continental basins and their petroleum potential in Qinghai–Xizang (Tibet) plateau with Lunpola Basin as example. In: *Contribution to the Geology of the Qinghai–Xizang (Tibet) Plateau*. Beijing: Geological Publishing House, **17**, 391–399 (in Chinese with English abstract).

Yang, X. S. (2002). Intracrustal partial melting and its significances, exemplified by Tibetan Plateau. Ph.D. dissertation, Institute of Geology, China Seismological Bureau, 109 pp.

Yin, A. & Harrison, T. M. (2000). Geologic evolution of the Himalayan–Tibetan orogen. *Annual Review of Earth and Planetary Sciences* **28**, 211–280.

Yin, A. & Nie, S. (1996). A Phanerozoic palinspastic reconstruction of China and its neighboring regions. In: Yin, A. & Harrison, T. M. (eds) *The Tectonic Evolution of Asia*. New York: Cambridge University Press, pp. 442–485.

Yin, A., Harrison, T. M., Ryerson, F. J., Chen, W. J., Kidd, W. S. F. & Copeland, P. (1994). Tertiary structural evolution of the Gangdese thrust system in southeastern Tibet. *Journal of Geophysical Research* **99**, 18175–18201.

Yin, A., Harrison, T. M., Murphy, M. A., Grove, M., Nie, S., Ryerson, F. J., Wang, X. F. & Chen, Z. L. (1999*a*). Tertiary deformation history of southeastern and southwestern Tibet during the Indo-Asian collision. *Geological Society of America Bulletin* **111**, 1644–1664.

Yin, A., Kapp, P. A., Murphy, M. A., Harrison, T. M., Grove, M., Ding, L., Deng, X. & Wu, C. (1999*b*). Significant late Neogene east–west extension in northern Tibet. *Geology* **27**, 787–790.

Yin, J., Xu, J., Liu, C. & Li, H. (1988). The Tibetan plateau: regional stratigraphic context and previous work. *Philosophical Transactions of the Royal Society of London* **327**, 5–52.

Zhang, S. Q. (1996). Mesozoic and Cenozoic volcanisms in central Gangdese: implications for lithosphere evolution of the Tibet Plateau. Ph.D. dissertation, China University of Geosciences, Beijing, 150 pp.

Zhao, W., Mechie, J., Brown, L. D., Guo, J., Haines, S., Hearn, T., Klemperer, S. L., Ma, Y. S., Meissner, R., Nelson, K. D., Ni, J. F., Pananont, P., Rapine, R., Ross, A. & Saul, J. (2001). Crustal structure of central Tibet as derived from project INDEPTH wide-angle seismic data. *Geophysical Journal International* **145**, 486–498.

Zhao, W. J., Nelson, K. D. & Project INDEPTH (1993). Deep seismic reflection evidence for continental underthrusting beneath southern Tibet. *Nature* **366**, 557–559.

Zheng, X. S., Bian, Q. T. & Zheng, J. K. (1996). On the Cenozoic volcanic rocks in Hoh Xil district, Qinghai Province. *Acta Petrologica Sinica* **12**, 530–545 (in Chinese with English abstract).

Zhou, D. & Graham, S. A. (1996). The Songpan–Ganzi complex of the West Qinling Shan as a Triassic remnant ocean basin. In: Yin, A. & Harrison, T. M. (eds) *The Tectonic Evolution of Asia*. New York: Cambridge University Press, pp. 281–299.

Zhou, S., Fang, N., Dong, G., Zhao, Z. & Liu, X. (2001). Argon dating on the volcanic rocks of the Linzizong group, Tibet. *Bulletin of Mineralogy, Petrology and Geochemistry* **20**, 317–319.

Zindler, A. & Hart, S. (1986). Chemical geodynamics. *Annual Review of Earth and Planetary Sciences* **14**, 493–571.